


3-24-2017

Mechanism of Cathodic Prevention of Carbon Steel in Concrete

Krittin Rattakham

University of South Florida, krittin@mail.usf.edu

Follow this and additional works at: <http://scholarcommons.usf.edu/etd>

 Part of the [Civil Engineering Commons](#), and the [Environmental Engineering Commons](#)

Scholar Commons Citation

Rattakham, Krittin, "Mechanism of Cathodic Prevention of Carbon Steel in Concrete" (2017). *Graduate Theses and Dissertations*.
<http://scholarcommons.usf.edu/etd/6630>

This Thesis is brought to you for free and open access by the Graduate School at Scholar Commons. It has been accepted for inclusion in Graduate Theses and Dissertations by an authorized administrator of Scholar Commons. For more information, please contact scholarcommons@usf.edu.

Mechanism of Cathodic Prevention of
Carbon Steel in Concrete

by

Krittin Rattakham

A thesis submitted in partial fulfillment
of the requirements for the degree of
Master of Science in Materials Science and Engineering
Department of Civil and Environmental Engineering
College of Engineering
University of South Florida

Major Professor: Alberto A. Sagüés, Ph.D.
Wenjun Cai, Ph.D.
Gray Mullins, Ph.D.

Date of Approval:
March 24, 2017

Keywords: Corrosion, Passive Film, In-situ Leaching,
pH Measurement, Chloride Threshold

Copyright © 2017, Krittin Rattakham

DEDICATION

This thesis is dedicated to my family members, including my father, my mother, my big sister, and my little brother. I have reached where I am thanks to their invaluable support and guidance.

ACKNOWLEDGMENTS

Special thanks, as well as gratitude, go to the following people and organization for their assistance throughout the project.

Distinguished Professor Alberto A. Sagüés, for giving me the opportunity to work in this extraordinary project and for being a great educator throughout the course of the project.

My colleagues, namely Hani Freij, Enrique Paz, and David Dukeman, for assisting me with many laboratory activities and above all, for keeping me accompanied for the duration of this project.

Florida Department of Transportation for funding this experiment. This work would not have been possible without the organization's financial support. Per agency request, a statement is made here to indicate that "The opinions, findings and conclusions expressed in this publication are those of the author and not necessarily those of the Florida Department of Transportation or the U.S. Department of Transportation".

TABLE OF CONTENTS

LIST OF TABLES.....	iii
LIST OF FIGURES.....	iv
ABSTRACT	vii
CHAPTER 1: INTRODUCTION.....	1
1.1 Background	1
1.2 Objective.....	2
1.3 Approach	3
CHAPTER 2: CORROSION AND ITS CONTROL IN CONCRETE.....	4
2.1 Chloride Attack of Reinforced Concrete	4
2.2 Chloride Threshold Dependency on Polarization Potential.....	5
CHAPTER 3: METHODOLOGY	7
3.1 Test Specimens Preparation	7
3.2 Polarization Levels	11
3.3 Wetting Conditions	11
3.4 Electrical Connections	12
3.5 Laboratory Environment	14
3.6 Polarization Measurements	15
3.7 EIS Tests	16
3.8 Exposure Termination	16
3.9 pH Measurements of Concrete Pore Water.....	17
3.10 Concrete Chloride Ion Concentration Measurements.....	21
CHAPTER 4: EXPERIMENTAL RESULTS AND DISCUSSION	22
4.1 Activation Sequence.....	22
4.2 Nominal Interfacial pH	24
4.3 Interfacial Chloride Ion Concentration	29
4.4 Visual Observations of Corrosion Damage.....	33
4.5 Summary Remarks on Extrinsic vs Intrinsic Mechanisms	34
CHAPTER 5: CONCLUSIONS.....	35

REFERENCES.....	36
APPENDIX A: LIST OF SYMBOLS.....	39
APPENDIX B: CHLORIDE ION CONCENTRATION MEASUREMENT.....	40
APPENDIX C: CHLORIDE ION CONCENTRATION CORRECTION.....	42
APPENDIX D: CONFIRMATORY NYQUIST PLOTS.....	48
APPENDIX E: CORROSION SPOTS ON ACTIVATED SPECIMENS	59
APPENDIX F: COPYRIGHT PERMISSION	66

LIST OF TABLES

Table 3.1 Summary of concrete mixture proportions.....	9
Table 3.2 Polarization level of the specimens	12
Table 4.1 Summary of the dates of activation and their respective t_A	24
Table 4.2 Summary of the measured nominal pH	28
Table 4.3 Summary of Cl^- concentration measurements.....	30
Table C.1 Summary of C_F values at the time of activation	46
Table D.1 Summary of the important EIS parameters.....	48
Table E.1 Summary of the corrosion spots size	59

LIST OF FIGURES

Figure 3.1 Dimensions and configuration of test specimen	9
Figure 3.2 Summary of specimen preparation sequence	10
Figure 3.3 Schematic of the potentiostat connection	13
Figure 3.4 Electrical connection and current flow direction of the circuits	14
Figure 3.5 Layout of the arrangement of the specimens	15
Figure 3.6 Example of the specimen demolition using a hydraulic press	17
Figure 3.7 Diagram showing location of the pond, front, and back surface	18
Figure 3.8 Schematic of the adapted ISL for pH measurement.....	20
Figure 4.1 Polarization history of the specimens.....	22
Figure 4.2 Plot showing exposure duration t_A of each specimen.....	23
Figure 4.3 Comparison of the average of nominal pH_F and pH_B	26
Figure 4.4 Nominal pH_F versus polarization voltage.....	27
Figure 4.5 Nominal pH_B versus polarization voltage	28
Figure 4.6 Development of C_S , C_F , and C_B with polarization voltage.....	31
Figure 4.7 C_T obtained from this experiment compared to other experiments	32
Figure 4.8 C_F/C_B ratio versus polarization voltage.....	33
Figure C.1 Diagram showing time lag between t_A and t_E	42
Figure C.2 Summary of the process to obtain C_{FA} from C_{FE}	46

Figure C.3 Plot of C/Cs versus normalized time.....	47
Figure D.1 Nyquist plot of the specimen C1, shown in a comparative scale	49
Figure D.2 Close-up look of the Nyquist plot of the specimen C1	49
Figure D.3 Nyquist plot of the specimen C5, shown in a comparative scale	50
Figure D.4 Close-up look of the Nyquist plot of the specimen C5	50
Figure D.5 Nyquist plot of the specimen C9, shown in a comparative scale	51
Figure D.6 Close-up look of the Nyquist plot of the specimen C9	51
Figure D.7 Nyquist plot of the specimen L2, shown in a comparative scale.....	52
Figure D.8 Close-up look of the Nyquist plot of the specimen L2.....	52
Figure D.9 Nyquist plot of the specimen L6, shown in a comparative scale.....	53
Figure D.10 Nyquist plot of the specimen L10, shown in a comparative scale.....	54
Figure D.11 Close-up look of the Nyquist plot of the specimen L10.....	54
Figure D.12 Nyquist plot of the specimen M3, shown in a comparative scale.....	55
Figure D.13 Nyquist plot of the specimen M7, shown in a comparative scale.....	55
Figure D.14 Nyquist plot of the specimen M11, shown in a comparative scale.....	56
Figure D.15 Close-up look of the Nyquist plot of the specimen M11	56
Figure D.16 Nyquist plot of the specimen S4, shown in a comparative scale	57
Figure D.17 Close-up look of the Nyquist plot of the specimen S4	57
Figure D.18 Nyquist plot of the specimen S8, shown in a comparative scale	58
Figure D.19 Close-up look of the Nyquist plot of the specimen S8	58
Figure E.1 Corrosion spots on the steel-concrete interface of specimen C1	60
Figure E.2 Corrosion spots on the steel-concrete interface of specimen C5.....	60
Figure E.3 Corrosion spots on the steel-concrete interface of specimen C9.....	61

Figure E.4 Corrosion spots on the steel-concrete interface of specimen L2	61
Figure E.5 Corrosion spots on the steel-concrete interface of specimen L6	62
Figure E.6 Corrosion spots on the steel-concrete interface of specimen L10	62
Figure E.7 Corrosion spots on the steel-concrete interface of specimen M3	63
Figure E.8 Corrosion spots on the steel-concrete interface of specimen M7	63
Figure E.9 Corrosion spots on the steel-concrete interface of specimen M11	64
Figure E.10 Corrosion spots on the steel-concrete interface of specimen S4	64
Figure E.11 Corrosion spots on the steel-concrete interface of specimen S8	65

ABSTRACT

In this work, I aim to clarify the mechanism that allows steel to attain higher chloride threshold as it is cathodically polarized. Specifically, I seek to provide empirical information on whether an intrinsic (predominantly interfacial effects of polarization) or an extrinsic (predominantly concentration changes due to polarization) mechanism may be dominant in the beneficial effect of polarization. I carried out this experiment with 12 identical concrete specimens, each with a cast-in steel plate, constantly exposed them to high-chloride environment. The specimens were divided into 4 triplicates and polarized at 4 different level from OCP, -200, -300 to -400 mV_{SCE}

The specimens were closely monitored for signs of corrosion. When corrosion was detected in a specimen, it was demolished to gain access to steel-concrete interface. Measurements of pH using a novel procedure and chloride ion concentration were done on the interface using an adapted in-situ pH measurement and a Florida Department of Transportation procedure respectively. The pH and chloride ion concentrations obtained in this study favor to some extent a dominant intrinsic mechanism interpretation, while the evidence in support of a dominant extrinsic mechanism interpretation remains elusive.

CHAPTER 1: INTRODUCTION

1.1 Background

Although often not posing an immediate danger, corrosion is the root cause of numerous cases of cumulative damage in metallic structures. It has been estimated ^[1] in 2013 that global economic damage due to corrosion was as high as 3.4 percent of the global Gross Domestic Product of the same year. These figures could have been higher if the damage to human lives and environment had been taken into account.

In Florida, where transportation via coastal bridges is a necessity, corrosion of carbon steel rebar in concrete structures supporting the bridges has proven to be a persistent problem. While carbon steel in the high pH concrete medium is capable of producing a metal oxide film (known as a passive film) that naturally prevents corrosion, this film can be easily broken down by the presence of chloride ion ^[2-3] from seawater. Those ions can be transported to the rebar surface via diffusion through the concrete pores. Steel corrosion ensues that creates expansive corrosion products that crack the concrete needing costly repairs.

The chloride content on the steel surface that, if exceeded, causes passive film breakdown is called the chloride threshold C_T ^[2, 4]. To combat this problem, the method known as Cathodic Prevention (C_{Prev}) has been employed to retard, and to some extent, prevent corrosion from ever happening. Cathodic Prevention involves supplying

electrons from an external source to the concrete reinforcement, often using impressed current, in such a way that the reinforcement becomes negatively charged with respect to the inert counter electrode (cathodic polarization) [6, 14]. It has been observed that the result is a significant increase in the value of C_T . Although it has been demonstrated that Cathodic Prevention can indeed increase the service life of rebar in concrete [5-6], there is relatively little information on the mechanism that is responsible for such effect.

It is possible to propose two alternatives regarding the possible mechanism. One states that in cathodically polarized rebar, the consequent flow of negative ions away from the steel includes the Cl^- that are in close proximity to the steel surface; thus helping to prevent passivity breakdown. Moreover, cathodic polarization promotes evolution of hydroxide ions, which increase local pH and promote passivity as well [7-10]. That combined effect of beneficial surface chemistry changes, will be referred to in the following as the extrinsic mechanism. The other explanation, that reflects experimental results from other studies [11-12], is that the impressed current triggers a beneficial change in the metal oxide film's properties (or in its ability to repair itself upon incipient damage), making it more resistant to chloride attack. That will be referred to in the following as the intrinsic mechanism. Those alternatives are of course extreme scenarios. It is not clear at present whether one of these two mechanisms may be dominant, and in that case, which one. This work is intended to address this issue.

1.2 Objective

The objective of this investigation is to provide empirical information on whether an extrinsic (predominantly concentration changes due to polarization) or an intrinsic (predominantly interfacial effects of polarization) mechanism may be dominant in the

beneficial effect of C_{Prev} application. In addition, we hope to further quantify the magnitude of this effect, to help determining how much polarization potential is needed to obtain a given effect.

1.3 Approach

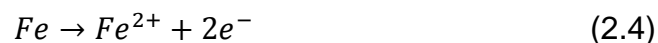
- The technical background of electrochemical corrosion and corrosion control phenomena in concrete was reviewed.
- Multiple specimens of concrete with an embedded steel plate were prepared and divided into 4 groups. One was free from polarization; the other 3 were cathodically polarized each at a different level.
- Each specimen was exposed to concentrated salt water at the surface closest to the steel plate.
- The specimens were closely monitored until corrosion of the steel plate was detected.
- When corrosion was detected, the steel plate was removed from the corroded specimen and the concrete immediately next to steel-concrete interfaces was examined for pore water pH and chloride content.
- The pH and chloride content at the concrete - steel interface of each specimen at the moment of steel activation were evaluated. The results were interpreted as to whether they supported either a preponderantly extrinsic or intrinsic cathodic prevention mechanism.

CHAPTER 2: CORROSION AND ITS CONTROL IN CONCRETE

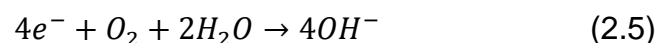
2.1 Chloride Attack of Reinforced Concrete

As established earlier in the introduction, chloride ions could severely deteriorate reinforced concrete structures. Typically, it is Cl^- from the service environment (e.g., seawater) that primarily contribute to the corrosion of rebar inside concrete.

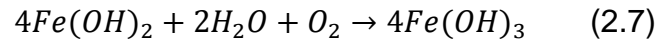
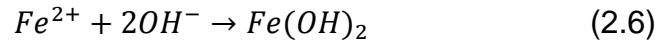
Although carbon steel is capable of developing a passive film when reacting with the highly alkaline products from concrete hydration, these films are vulnerable to chloride attack for reasons not yet perfectly understood. On exposure to seawater, chloride ions are transported from outside through the concrete pores via diffusion [13-14]. Given enough time, these chloride ions can accumulate on rebar surface until they reach a high enough concentration to break down the passive film on steel. This maximum allowable concentration of chloride ions is referred to as the 'Chloride Threshold' or C_T . When the passive film is damaged and the underlying steel is exposed to the pore water, an electrochemical cell is established. The corrosion of carbon steel (which is mostly Fe) in pore water is an electrochemical reaction, which can be broken down into partial reactions as follows [15]. one is an anodic reaction:



The other is a cathodic reaction that can be expressed as follows.



The Fe ions from the anodic reaction leave the rebar and react with hydroxide ions, water, and oxygen to form corrosion products as follows.



These corrosion products, $Fe(OH)_3$ and $Fe(OH)_2$, have higher volume than that of iron. When these products accumulate inside concrete, the concrete experiences expansion stresses which may cause the concrete to crack. Later on, the corroded rebar loses its load-bearing capability over time, which could eventually result in steel failure. These events are highly undesirable from an engineering standpoint.

2.2 Chloride Threshold Dependency on Polarization Potential

A number of researches have been conducted to determine factors that could influence C_T of rebar in concrete and how can those factors be altered to prolong the service life of concrete structures. It has been shown that factors such as increased temperature, presence of sulfates, and tidal condition have detrimental effect on C_T , while factors such as C_3A content, water-to-cement ratio (w/c), and concrete cover thickness may affect the value of C_T in various ways [12, 16-17]. Also, C_T increases if the concentration of (beneficial) OH^{-} ions in the pore water is increased [18]. In particular, it has been found that polarizing the reinforcing steel in the cathodic direction could substantially increase C_T . The initial work by Alonso et al. [19] shows that polarization at a potential more cathodic than $-200 \pm 50 \text{ mV}_{SCE}$ increases C_T of the concrete reinforcement by roughly 3 times. The trends were further confirmed by Sanchez [20], as it was found in her study that there was a trend of increasing C_T as cathodic polarization increased. In the work by Dugarte and Sagüés [21] to study C_T dependence of rebar in cracked concrete exposed to a simulated

marine environment, it was reported that there was an improvement of C_T value when the specimens were cathodically polarized at -430 mV or more. However, the precise mechanism behind the beneficial effect of cathodic polarization voltage has on C_T of steel in concrete is still unknown at large.

As noted earlier, there are two possible extreme interpretations concerning the mechanism responsible for such effect. The first interpretation (extrinsic mechanism) states that the threshold increases mainly because Cl^- were locally carried away by the electric field imposed to polarize the steel, aided by the local enrichment in OH^- ions (increased pH) generated by the cathodic reaction. Experimental evidence supporting this hypothesis would involve finding significantly higher pH values, and relatively lower or less changed chloride ion content in the concrete pore water immediately next to the cathodically polarized steel-concrete interface when corrosion finally starts. The other hypothesis (intrinsic mechanism) states that the cathodic polarization mainly modifies properties of the passive film, improving its resistance to chloride-induced breakdown. Local Cl^- and pH changes would be playing only a minor role. Evidence supporting this alternative would include observation of greater Cl^- content near the interface when corrosion finally occurs in increasingly cathodically polarized steel, without indications of strong increases in local pH. Tests of the extent to which either mechanism may be predominant are conducted in the present investigation.

CHAPTER 3: METHODOLOGY

3.1 Test Specimens Preparation

To simulate conditions of a steel-reinforced concrete structure in marine service, twelve identical concrete specimens were created and exposed to a high chloride environment. Each specimen had an acrylic pond built on the top side, a carbon steel plate embedded in the center, and an activated titanium rod inserted between the plate and the pond. The specimen's dimension and configuration are shown in Figure 3.1.

The ponds were made to contain a concentrated sodium chloride solution, which would represent the high-chloride environment an actual concrete structure has to experience. The steel plates were used in place of rebar as they have a well-defined flat surface, allowing pH measurement and concrete sampling at the steel-concrete interfaces to be done easily. An activated titanium rod was included in every specimen, centered ½" above the steel plate to serve as an instrumentation control reference electrode for the electrochemical cell. Actual potential measurements and calibrations were made against a Saturated Calomel Electrode (SCE) temporarily placed on the pond as described later.

The concrete mixture proportions are shown in Table 3.1. The mixture consisted of limestone as coarse aggregate, sand as fine aggregate, and Portland cement paste. The cement-to-water (w/c) ratio was 0.5. This was to ensure that the resulting concrete

would be permeable enough to permit steel - Cl⁻ interaction to take place within a reasonably short amount of time. The specimen preparation sequence is summarized in Figure 3.2. The concrete was mixed in a rotary concrete drum mixer, and then cast into wooden molds that had a steel plate and an activated titanium rod fixed in position. During casting, air pockets were prevented using a combination of a vibrating table, hitting with a rubber mallet, and frequent rodding. Afterward, the molds were adequately sprayed with tap water before being wrapped under plastic sheets. The wrapped concrete-filled molds were kept for 5 days in laboratory air. At the end of that period there were some visual signs of shrinkage, possibly due to water absorption by the wooden mold walls in spite of prior application of mineral oil as mold release. Accordingly, the specimens were then immediately removed from the molds and placed inside a 100 percent humidity chamber to continue curing. During the subsequent period of 20 days, the specimens were periodically sprayed with tap water to maintain the hydration process. Afterwards, the specimens were removed from the curing chamber and exposed to laboratory air while the ponds, sides and wiring were processed as indicated below.

The 3.2 mm thick steel plates were used in the as-received condition, with the original surface mill scale in place, simulating a usual rebar condition. Each of them was engraved for identification. The part of the steel that emerged from the concrete was protected from localized corrosion by an epoxy coating strip for about 8 mm on each side of the emersion line. The surface area of steel in contact with concrete and facing the pond (disregarding edges) was 140 cm²; an equal area of steel in contact with concrete was facing downwards.

Table 3.1 Summary of concrete mixture proportions

Mixture Proportions		
Component	Value	Units
Portland Cement Type VIII	395	kg/m ³
Coarse Aggregate (Limestone)	908	kg/m ³
Fine Aggregate (Silica Sand)	794	kg/m ³
Water-to-Cement Ratio	0.5	
Water	198	kg/m ³
Expected Density of Concrete	2295	kg/m ³

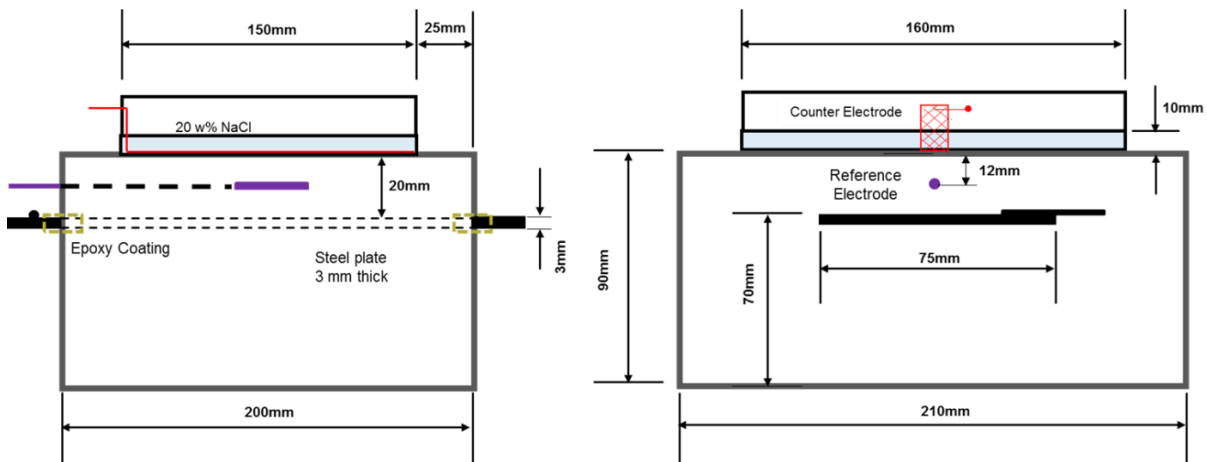


Figure 3.1 Dimensions and configuration of test specimen

The ponds used to contain sodium chloride solution on top of each specimen were made of Plexiglas panels, machined to have the desired dimension as shown Figure 3.1. Four Plexiglas panels were glued together with acrylic cement to form a rectangular frame. After 12 frames had been created, they were then glued to their respective specimens using JB-Weld® epoxy on the contact edges. Leak tests were performed by

filling the pond with tap water to a 30 mm height and applying a paper towel on the seam area to confirm that there was no leakage.

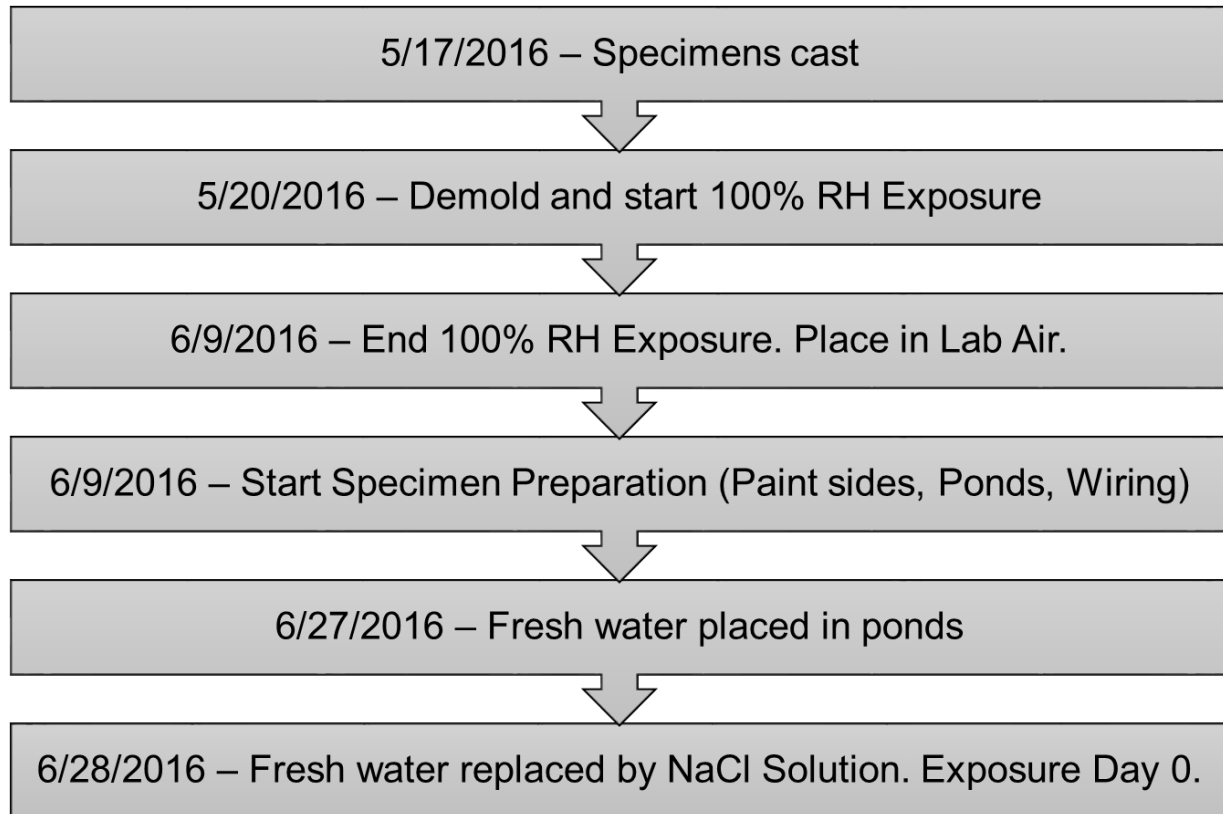


Figure 3.2 Summary of specimen preparation sequence

The top surface of the each specimen, except for the pond area, was coated with Sikadur®32 epoxy coating of approximately 1 mm thickness while the side surfaces were painted with Clark+Kensington paint+primer® to prevent side evaporation and ensure maximum one-dimensional diffusion from the pond solution to the plate.

Lastly, a counter electrode made of an activated titanium mesh ribbon, 1.5 cm wide, was installed in the pond in such a way that the majority of the strip would lay on the pond's bottom while the rest was bent upward and remained above water level to make a contact there as demonstrated in Figure 3.1. Each counter electrode strip had a stainless steel wire spot-welded to it to serve as a connection to the wires to the control box. The above-water end of the electrode was glued to the Plexiglas panel and the end of the submerged portion was glued to the pond surface with JB Kwik™ epoxy.

3.2 Polarization Levels

The twelve specimens were split into four groups of three each. Three groups were cathodically polarized at levels of -200, -300, and -400 mV_{SCE}, while one group, was left at the open circuit potential (about -100 mV_{SCE}). These conditions were designated each by a letter: L, M, S and C for Low, Medium, and Strong polarization as well as Control respectively. The summary of the specimens and their respective polarization level are presented in Table 3.2.

3.3 Wetting Conditions

The specimens were exposed to fresh water in the pond for a brief conditioning period as detailed in Figure 3.2. The fresh water was then replaced with a 20 weight percent NaCl solution. The solution was prepared by measuring 500 grams of dry NaCl salt, transferred them into a 2 liters volumetric flask, then adding distilled water until the solution level reached the 2 liters mark and thoroughly agitated. The solution was carefully poured into each specimen's pond. The water level was kept between 8 to 9 mm, as measured from the pond's bottom. Pond lids were made of Styrofoam® of ¾" thickness

Table 3.2 Polarization level of the specimens

Group C		Group L		Group M		Group S	
Specimen No.	Open Circuit Potential (mV _{SCE})	Specimen Name	Polarization Level (mV _{SCE})	Specimen No.	Polarization Level (mV _{SCE})	Specimen No.	Polarization Level (mV _{SCE})
C1	Typically -80 to -100	L2	-200	M3	-300	S4	-400
C5		L6		M7		S8	
C9		L10		M11		S12	

*A nominal value of -100 mV_{SCE} was chosen for graphic representation of results from this group

to retard water evaporation and maintain the intended chloride concentration throughout the experiment. Exposure to the chloride solution started on 6/28/2016, designated as Day 0 of the exposure period. Exposure duration is hereafter counted in days from this date.

3.4 Electrical Connections

Every specimen, except for those in the group C, was controlled via two 6-channels potentiostats, which regulated the voltage between each specimen's steel plate and the counter electrode. The connection schematic of the potentiostat used in this experiment is shown in the Figure 3.3. Each channel of the potentiostat was configured to maintain a fixed value of voltage across the working and reference terminal; current would thus be drawn from the power supply through neural terminal to maintain that voltage.

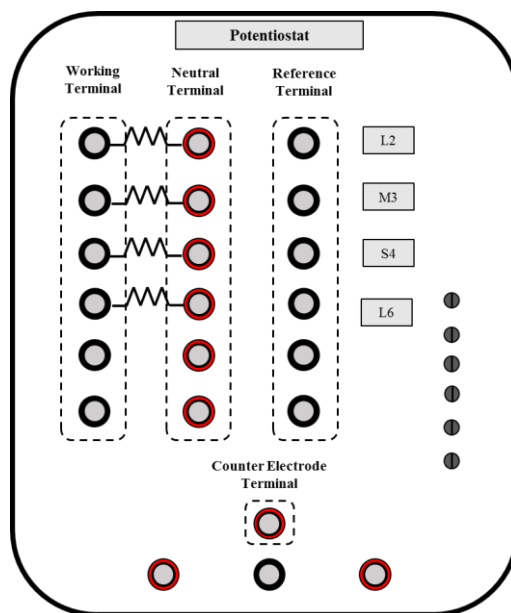


Figure 3.3 Schematic of the potentiostat connection

The connections between each specimen and its respective potentiostat channel were established using copper wires in such a way that steel plates were negatively polarized, as intended for cathodic polarization. Therefore, during the experiment, the polarized specimens were constantly experiencing conventional current coming into the counter electrode and exiting through steel plate back to the potentiostat as shown in Figure 3.3.

Additionally, a diode was inserted as shown in each polarized specimen circuit, to prevent any anodic polarization current to flow after activation of the steel occurred. That way, disruption of the just-activated specimens immediately after spontaneous activation was avoided, so the conditions at the interface experienced minimum disturbance prior to specimen demolition and characterization.

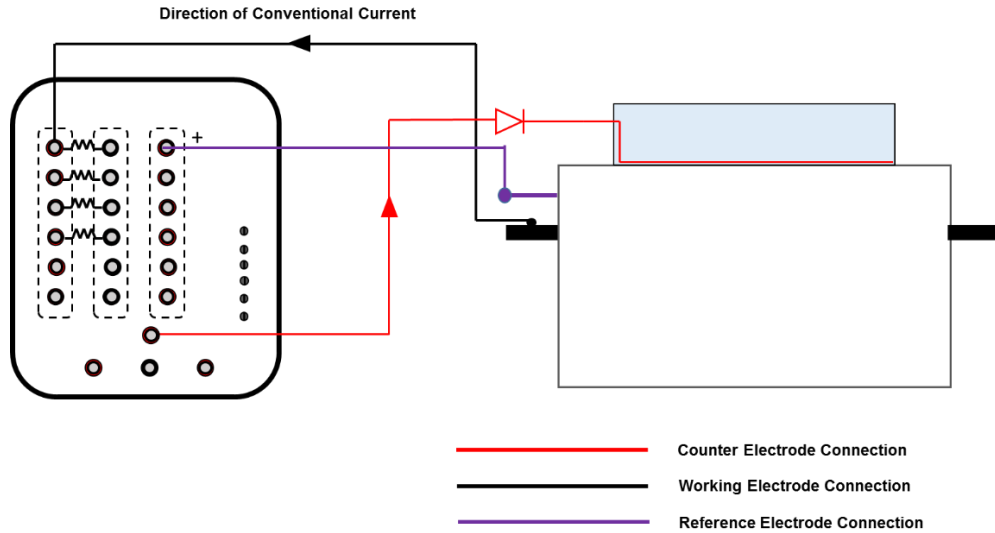


Figure 3.4 Electrical connection and current flow direction of the circuits

3.5 Laboratory Environment

All the apparatuses and the specimens were placed on top level of a shelf situated in the western part of the corrosion lab. The specimen and equipment layout (avoiding grouping by polarization level so as to minimize systematic disturbances) is displayed in Figure 3.5. The lab was air-conditioned and had temperature between 22.5 and 24 degree Celsius throughout the period of experiment.

Despite the Styrofoam[®] lids covering the ponds, as the relative humidity inside the lab was 60% the pond solution of the specimens evaporated somewhat over time. For this reason, it was necessary to periodically restore the pond solution with deionized water to maintain the initial water level and NaCl concentration. Checks of the solution conductivity performed on samples extracted at the time of specimen activation confirmed that the solution concentration remained close to the nominal 20% NaCl initial amount (coefficient of variation $\approx 8\%$).

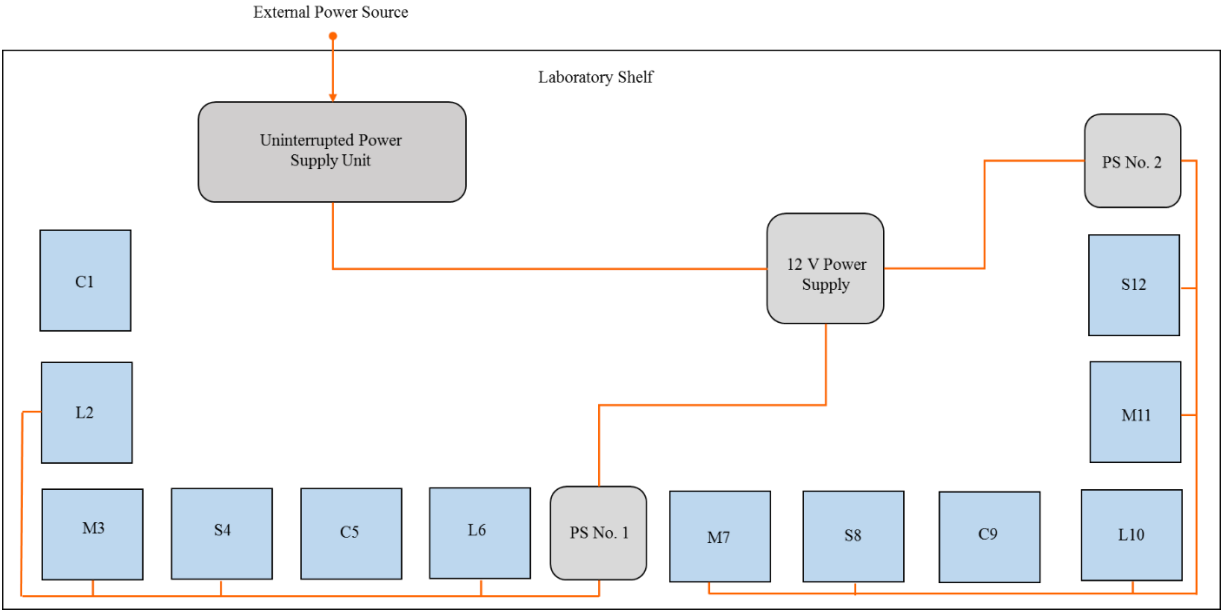


Figure 3.5 Layout of the arrangement of the specimens

3.6 Polarization Measurements

A Fluke® multi-meter Model 289 was used to measure and record the polarization voltage between steel plate and activated titanium reference electrode, steel plate and SCE, and the current being consumed by each specimen to maintain the desired voltage. The voltage between steel plate and reference electrode was not measured directly on the specimens but instead by connecting the multi-meter's positive probe into working electrode terminal (W) and the negative probe to the reference electrode terminal (R) on the potentiostat. Potential versus SCE was measured by submerging an SCE tip into salt solution while connecting the negative probe of the multi-meter to the SCE electrode and the positive probe to steel plate. The polarization current was measured as a voltage across a 1kΩ shunt resistor between the neutral and the working terminal of each channel. This voltage was later converted to current using Ohm's law. This voltage was

called I^*1000 voltage to indicate its relationship with current and the $1k\Omega$ resistor. The potential versus reference electrode and SCE were recorded in mV, while the potential versus SCE were recorded as mV_{SCE} .

When a drop in the OCP potential of a control specimen versus SCE had been detected, that specimen was flagged as suspected of activation, since this potential drop is usually associated with passive film breakdown in carbon steel. For polarized specimens, the specimen was flagged as suspect of activation if the polarizing current went to zero. Due to the diode in the circuit, activation of the polarized specimens also meant that they transitioned to an open circuit condition with a potential more negative than the target polarization potential of the specimen). The flagged specimen was then investigated further with Electrochemical Impedance Spectroscopy (EIS) to verify its state of activation.

3.7 EIS Tests

Shortly after a significant drop in voltage versus SCE, along with I^*1000 voltage becoming zero has been detected in a specimen, a potentiostatic EIS test at the open circuit condition was conducted using a Reference Potentiostat, Model 600 by Gamry®. If the Nyquist plot obtained from the test was indicative of corrosion, the specimen was declared to be under activation condition. The exposure period at which the confirmatory EIS test was conducted, counting from day zero, was designated as the activation time t_A for that specimen.

3.8 Exposure Termination

Shortly after it was determined that a specimen's reinforcement had reached the active condition, the specimen was disconnected from the control circuit and the pond

solution was immediately removed from the pond and stored for later analysis in an airtight plastic container. The exposure period at the time of pond solution removal was designated as t_R . The specimen pond surface was blotted dry, lightly rinsed with fresh water to remove any solid salt crystals and then blow-dried. The concrete on the pond surface was then milled for powder samples. The exposure duration at the day of powder sample extraction was designated as t_E . The specimen was then immediately demolished as detailed in Figure 3.6. The concrete pieces were kept in a chamber at 100% RH and periodically removed to do pH measurements and later on, concrete powder extraction of the remaining interfaces for chloride concentration measurements.



Figure 3.6 Example of the specimen demolition using a hydraulic press

3.9 pH Measurements of Concrete Pore Water

Specimens were demolished to remove the embedded steel plate and have both of its steel-concrete interfaces analyzed for pH using a newly implemented variation of

the in-situ leaching method (ISL) [24], adapted to be used on a flat surface and without having to drill holes on a specimen. The bottom of the pond was referred to as the “pond surface”, the upper steel-concrete interface as the “front surface”, and the lower steel-concrete interface as the “back surface”. The position of those surfaces is shown in Figure 3.7. This nomenclature shall be used throughout this report.

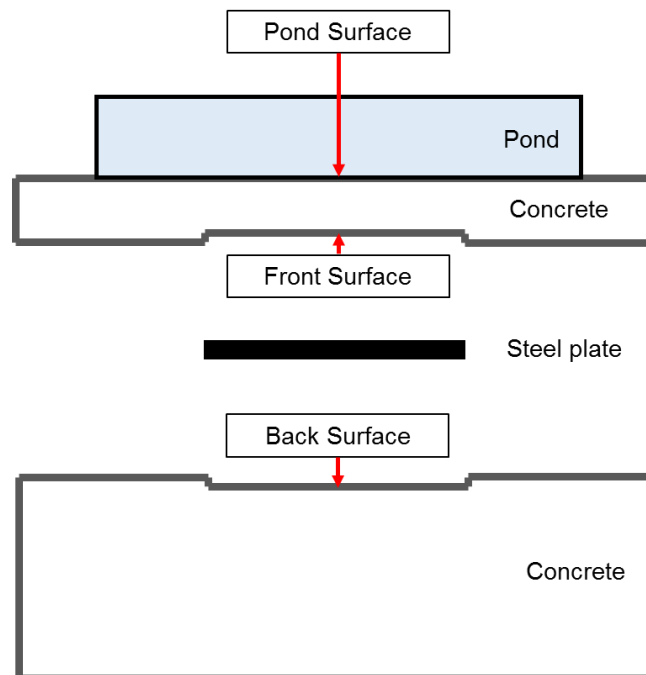


Figure 3.7 Diagram showing location of the pond, front, and back surface

To obtain a sample of concrete pore water near a steel-concrete interface, 16 pieces of filter paper (Whatman® no.41, 47 mm-diameter) were prepared, 8 large pieces and 8 small pieces.. All the 16 pieces were oven dried at 110 C for at least 10 minutes. The smaller papers, called sampling papers, were weighted down to 0.00001 gram precision. Following the drying process, the bigger filter papers were dipped in distilled water and then gently placed on the concrete interface to be examined. These bigger filter

papers were used as a base to prevent the sampling papers from being contaminated by concrete dust on the interface. The sampling papers were then dipped in distilled water and placed on top of the base papers as demonstrated in Figure 3.8. The papers were covered under a sheet of clean Saran™ wrap to prevent water evaporation and air contamination. Pieces of soft dry sponge were then placed on top of the Saran™ wrap, followed by a flat object heavy enough to press the filter papers against the concrete interface.

The specimen and its filter papers were kept inside a 100% RH chamber for at least 20 hours to allow enough time for concrete pore water to mix and equilibrate with the water in the sampling papers. Some of the water in the papers was expected to have been absorbed in the concrete pores as well, following processes described elsewhere [24]. Separately, plastic vials were filled with 0.5 ml of distilled water and accurately weighed. At the end of the soaking period, each sampling paper was taken out of the concrete specimen and placed inside a separate designated vial. The total weight of each vial plus soaked sampling paper yielded by difference from the previous records the mass of extracted pore water-equilibrated sample.

The diluted pore water solution contained in each vial was analyzed for pH using a solid state pH sensing microelectrode. The procedure consisted of three steps. In the first the pH electrode was calibrated against standard buffer solutions ranging from pH 8 to 13. Calibration was repeated until verifying that a potential slope of 57 ± 3 mV per 1 pH point increment was obtained.

The second step was to measure the potentials of the diluted concrete pore water samples and compare them to that of pH buffer solutions. Starting with the diluted

concrete pore water sample, the electrodes of the successfully calibrated pH meter were submerged into the sample for 30 seconds. The potential reading at the end of this period was recorded. Based on this potential, two buffer solutions were selected, one that gave a potential reading just above the sample's potential and the other just below it. Both buffer solutions were measured for potential at the 30 seconds mark following the diluted pore water sample. This procedure was repeated until 3 potentials were obtained for each solution involved.

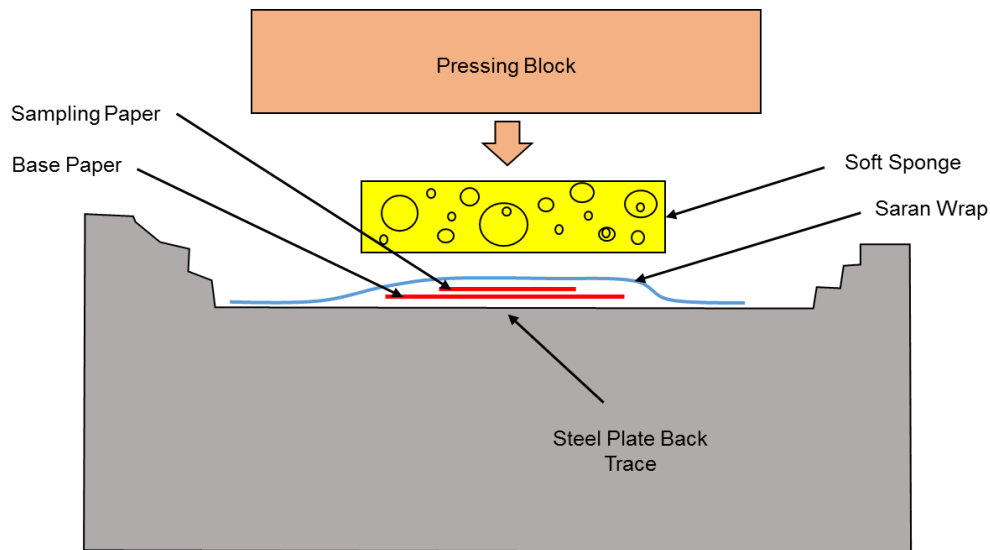


Figure 3.8 Schematic of the adapted ISL for pH measurement

The final step was to determine the pH of the actual concrete pore water. The data obtained in the second step were plotted in a potential versus time format using Microsoft Excel ®. The linear equation of each solution was obtained; resulting in three linear equations that described how the potentials of the sample and the two buffer solutions fluctuated over the measurement period. Each equation was used to calculate the

potentials of their respective solution at the beginning of the measurement, half way through the measurement, and at the end of the measurement. Since the pH values of the two buffer solutions were known, the pH of the diluted pore water sample was obtained through linear interpolation for each of the three times. The value of the pH of the solution was reported as the average of those three values. By taking into account the dilution factor (the ratio of total water mass inside the tube to mass of the absorbed pore water), a nominal pH value of the actual concrete pore water was obtained. This nominal estimate did not take into account possible variation of the activity coefficient with concentration of OH⁻ ions. Future work will attempt to refine the estimate by incorporation of that factor.

3.10 Concrete Chloride Ion Concentration Measurements

Concrete Chloride ion measurement was performed to determine Cl⁻ concentration at the time of activation at the three surfaces of every concrete specimens. The surfaces at which the Cl⁻ concentration were obtained included the pond surface, the front surface, and the back surface, as identified in Figure 3.7.

This test was adapted from FDOT method, the FM5-516: Standard for Determining Low-Levels of chloride in Concrete and Raw Materials ^[25]. The samples were prepared by milling the appropriate surfaces of the specimens for powder. The exposure period at the moment of powder extraction is designated as t_E . These powder samples were then analyzed for their Cl⁻ concentration as detailed in Appendix B.

CHAPTER 4: EXPERIMENTAL RESULTS AND DISCUSSION

4.1 Activation Sequence

Consistent with section 3.6, the exposure duration was recorded in days, counted from Day 0. Figure 4.1 summarizes the polarization history of the test specimens and the related activation events as explained also in section 3.6.

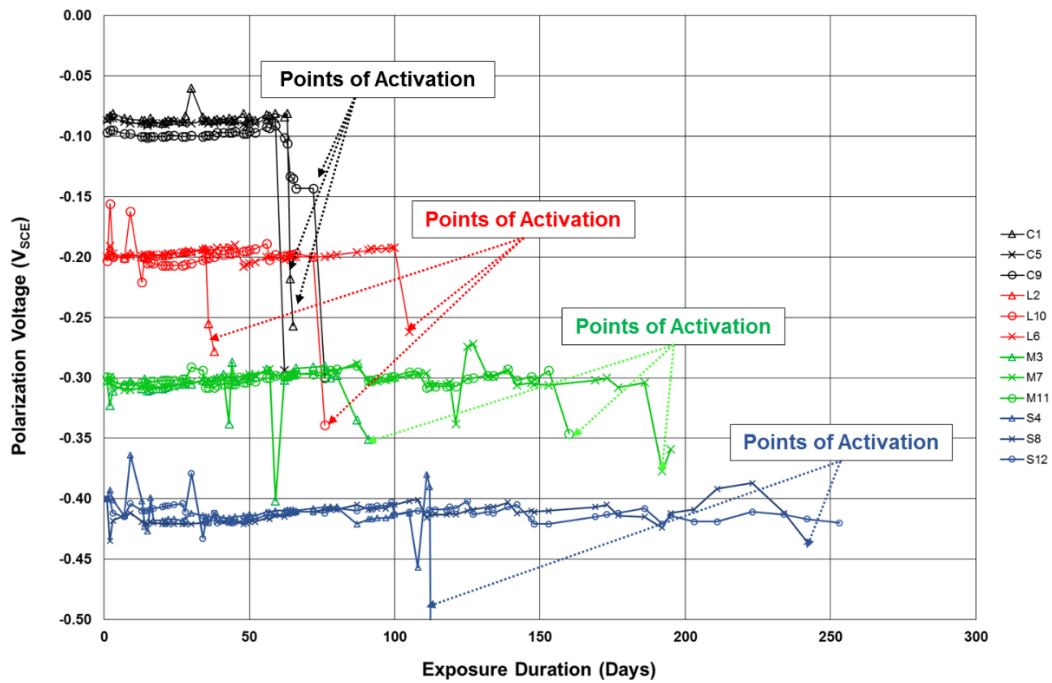


Figure 4.1 Polarization history of the specimens. Black, Red, Green and Blue traces correspond to specimen types C,L,M and S respectively.. See Table 4.1 for details.

Table 4.1 summarizes the t_A values of each specimen, shown in chronological order. Figure 4.2 is a graphic representation of the same data, with the addition of average values of t_A of specimens of the same polarization condition. As can be seen, although with some scatter, there was a clear increase in t_A as the potential became more cathodic. This trend is consistent with the expectation that cathodic polarization provides beneficial effects on which the principle of cathodic prevention is based.

It should be noted that, surprisingly, specimen L2 that was polarized at $-200 \text{ mV}_{\text{SCE}}$ was the first to display signs of activation. After specimen L2 was declared active, specimens C5, C1, L10, C9, M3, L6, S4, M11, M7 and S8 began to activate in chronological fashion while S12 remains passive to this writing.

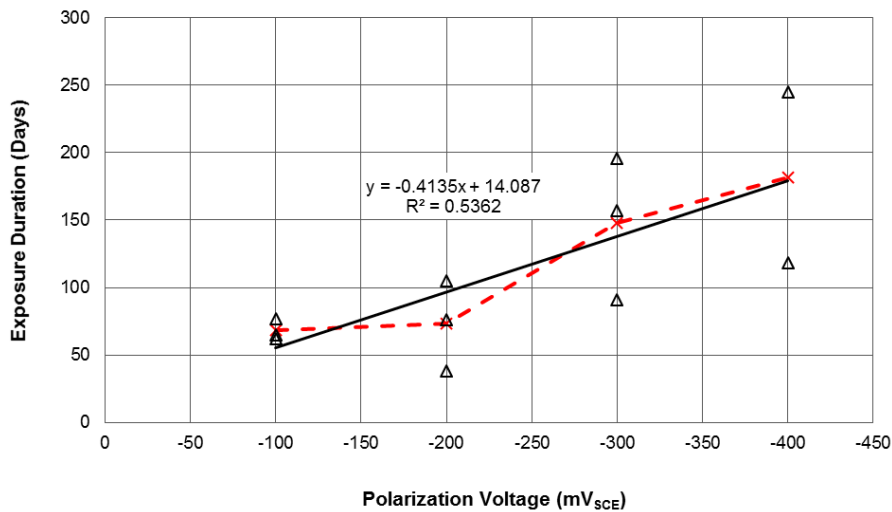


Figure 4.2 Plot showing exposure duration t_A of each specimen. The red dash line represents the average t_A of specimens of same polarization condition. Trend line included for visual speculative evaluation but no functional relationship is implied.

Table 4.1 Summary of the dates of activation and their respective t_A .

Specimen No.	Activation Date	t_A (Days)
L2	8/5/2016	38
C5	8/29/2016	62
C1	9/1/2016	65
L10	9/12/2016	76
C9	9/13/2016	77
M3	9/27/2016	91
L6	10/11/2016	105
S4	10/24/2016	118
M11	12/2/2016	157
M8	1/10/2017	196
S8	2/28/2017	245

4.2 Nominal Interfacial pH

The newly implemented ISL method provided amounts of filter paper pore-water equilibrated fluid (PE) mass typically in the order of ~5 mg, yielding ~100X dilution into the 0.5 cc vial solution. Samples so small so that dilution was >400X were deemed not viable for meaningful analysis and the corresponding results not used. Likewise any sample with PE mass > 100 mg was deemed to be suspect of insufficient equilibration with the pore water during the test interval and also not considered for evaluation. Those exclusions affected only ~10% of the total number of samples obtained; results for the remaining, qualified samples are summarized in Table 4.2, presenting also average pH values for the front and back sides in each case where available. Figure 4.3 shows comparisons between the average value of front- and back- pH_F and pH_B values respectively obtained from each specimen, while Figures 4.4 and 4.5 show all the measured pH_F and pH_B values versus polarization voltage.

Concrete pore water pH is often found to be in the pH 13-13.5 range [12, 24, 26] but as shown in the table and figures the present nominal values were on average in the upper part of the pH 13 range and in about 1/3 of the cases above pH 14. Taking those results at face value first, the data in Figure 4.3 do not show as a whole any clear consistent differentiation, emerging above the data scatter, between the front and back nominal pH values. Figure 4.4 hints at a slight increase in pH_F as cathodic polarization voltage increases but the scatter of the results is too great to identify that trend with confidence for the front interface. Likewise the data in Figure 4.5 for pH_B do not suggest any clear effect of polarization on nominal interfacial pH on the back side.

Given this lack of differentiation between front and back measurements, it may be assumed that the highest levels and duration of cathodic polarization used in the present experiments did not strongly increase the nominal interfacial pH of the front interface (which would have experienced the brunt of the polarizing current coming from the counter electrode) compared with that of the expectedly much less polarized back surface. The lack of strong differentiation between the values at either interface obtained for the various polarization levels further suggests that the polarization conditions used here did not strongly alter interfacial pH. Consequently, the results do not provide supporting evidence of a highly dominant extrinsic mechanism being at play in the conditions examined.

Some caveats on the above conclusion merit consideration however. The first concerns the general level of values of the nominal pH results obtained. If indeed those values do not reflect any interfacial polarization effect, it could be assumed that the values would be representative of the bulk pore water pH of the concrete. While measurements

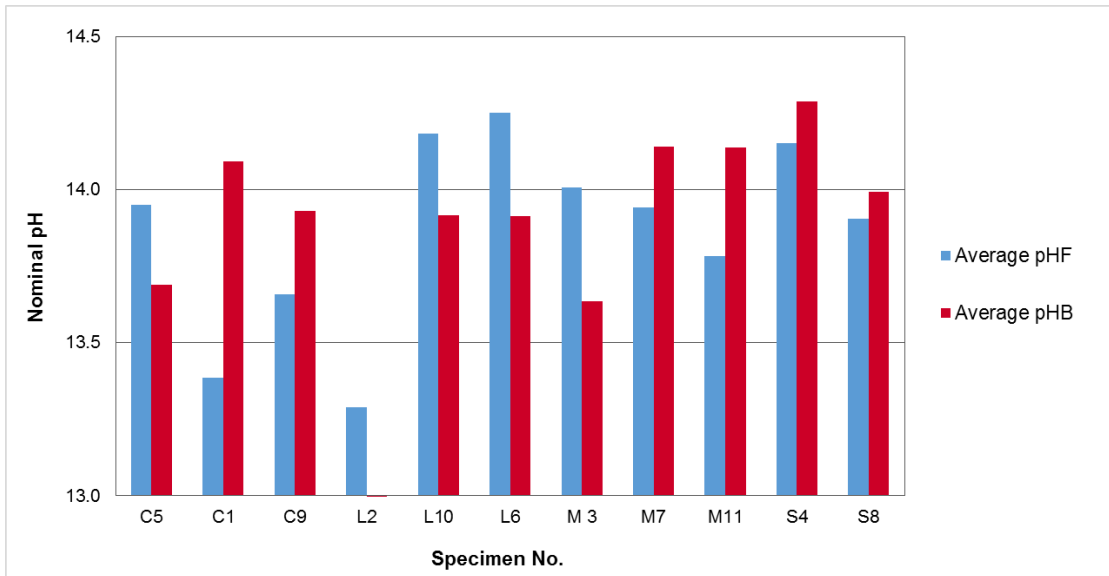


Figure 4.3 Comparison of the average of nominal pH_F and pH_B. C , L and, M and S correspond to open circuit conditions and the Low, Medium and Strong Polarization levels respectively as detailed in Table 3.2. Specimen L2 did not yield usable pH data for the Back surface. As of this writing only data for two of the S level specimens are available.

of the water pH in the bulk of this concrete by means of conventional ISL are not yet available, as noted above the values obtained here are about ~> 0.5 pH point greater than usually anticipated, suggesting some kind of systematic exaggerating artifact in the method used. This exaggerating effect may be in part due to systematic deviations such as measuring the concentration of OH⁻ (when diluted) at a higher activity coefficient [27] than when concentrated in the actual pore solution. It is possible also that there is some evaporative water loss between the moment the filter paper is removed from the concrete and when placed in the vial, falsely increasing the dilution factor and consequently the estimated nominal pH as well. Examination of these and similar possibilities is being conducted in follow-up work. In any event, these systematic factors are likely to have applied to all the measurements in about the same manner, so the relative meaning of the front-to-back and polarization effect findings noted above may still apply with some

reasonable confidence. A second concern is about the time evolution of the specimen between the moment when the polarization is stopped and the moment, after demolishing of the specimen when the nominal interfacial pH is finally assessed. In that interval any kind of compositional gradient created in the concrete next to the specimen is expected to undergo some relaxation, with consequent decrease in any pH differentiation. Such relaxation would occur also with Cl⁻ concentration gradients, but given the relatively fast diffusivity of OH⁻ ions compared to that of Cl⁻ ions the effect could be relatively more important in the first. The possible relevance of this issue is also to be examined in ongoing and follow-up modeling work for these systems. Pending those further analyses, the significance of the lack of strongly supporting evidence for an extrinsic mechanism noted in this work must be considered accordingly with caution.

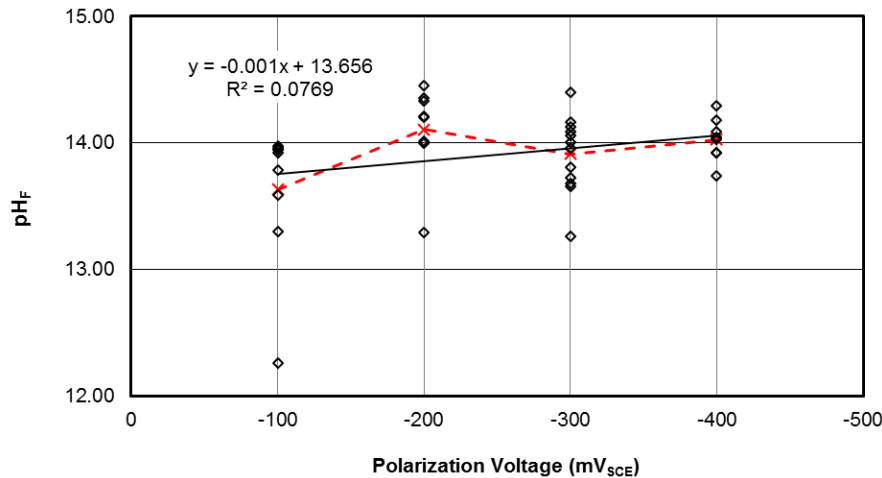


Figure 4.4 Nominal pH_F versus polarization voltage. Trend line included for visual speculative evaluation but no functional relationship is implied.

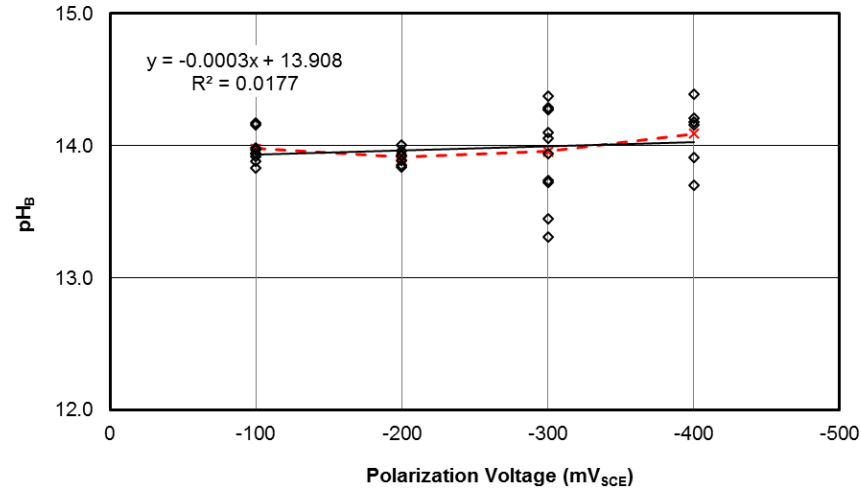


Figure 4.5 Nominal pH_B versus polarization voltage. Trend line included for visual speculative evaluation but no functional relationship is implied.

Table 4.2 Summary of the measured nominal pH

Summary of Nominal pH															
Polarization Potential (mV _{SCE})	Polarization Level	Specimen No.	t _A (Days)	Nominal pH _F (Sample E-F)				Average pH _F	Nominal pH _B (Sample A-D)				Average pH _B	Avg pH _F -Avg pH _B	C _{OHF} /C _{OHB}
				E	F	G	H		A	B	C	D			
-100 (OCP)	C	C5	62	-	-	13.9	14.0	14.0	-	13.3	13.8	14.0	13.7	0.26	1.82
-100 (OCP)		C1	65	-	14.0	13.9	12.3	13.4	-	14.2	13.9	14.2	14.1	-0.71	0.20
-100 (OCP)		C9	77	14.0	13.6	13.8	13.3	13.7	13.9	14.0	13.9	13.9	13.9	-0.27	0.54
-200	L	L2	38	-	-	13.3	-	13.3	-	-	-	-	-	-	-
-200		L10	76	-	14.3	14.2	14.0	14.2	-	13.9	14.0	13.9	13.9	0.27	1.85
-200		L6	107	14.0	14.4	14.5	14.2	14.3	13.9	14.0	13.9	13.8	13.9	0.34	2.17
-300	M	M3	91	13.8	14.4	14.2	13.7	14.0	13.7	14.1	13.4	13.3	13.6	0.37	2.35
-300		M7	195	13.7	14.0	14.1	14.0	13.9	13.7	14.3	14.3	14.3	14.1	-0.20	0.63
-300		M11	157	13.3	13.7	14.1	14.1	13.8	-	14.1	14.4	13.9	14.1	-0.35	0.44
-400	S	S4	118	14.0	14.1	14.2	14.3	14.2	-	-	14.4	14.2	14.3	-0.14	0.73
-400		S8	246	14.0	13.7	13.9	13.9	13.9	14.16	14.2	13.9	13.7	14.0	-0.09	0.81

4.3 Interfacial Chloride Ion Concentration

The data obtained from Cl^- concentration measurements are shown in Table 4.3. The Cl^- concentrations measured at the pond, front, and back surfaces were designated as C_S , C_F (corrected as detailed in Appendix C), and C_B respectively. The C_B measured initially obtained from specimen L2, 0.45 kppm, was deemed to be an outlier as this specimen was the first to activate and the measurement method was not yet optimized at that time, and only 0.5 grams of powder sample were available for the analysis. Instead, the value of C_B was estimated as being equal to the average value of the C_B values of the other two specimens from group L. That approximation assumed implicitly that concentrations on the back side would not be affected strongly by any polarization-related field due to the anticipated low current density on the back side.

As of this writing full chloride data were available for only one for the S specimens (of the three only two had activated, and chloride analysis for one of the latter had only been conducted for the pond and front surfaces). Nevertheless, some overall trends may be identified based on the combined results for all specimens, plotted as a group in Figure 4.6 as function of polarization level. The red dashed lines represent the average values of chloride ion concentration of the specimens with the same polarization voltage. Chloride content of the concrete at the pond surface showed considerable scatter but in general was high (about 12 kppm) , and consistent with contact with a 20 wt% NaCl solution, more than half way toward saturation ^[20,21].

Results for the front steel surface were similarly affected by scatter and relatively high on average for the control specimens (~4,000 concrete wt. ppm), for which a conservatively estimated chloride threshold of ~0.5 percent of the cement content (~1,000

concrete wt. ppm per Table 3.1) might have been estimated. The C_F values upon activation for the L group were not much different (and even slightly smaller on average) from those of the C group. Assuming that the beneficial effect of the $-200 \text{ mV}_{\text{SCE}}$ polarization was not much significant, and considering the C and L specimens as a group, the group has a scattering of results with a lower limit of 1,000 wt ppm. Viewed that way, the results are not inconsistent with expectations based on a conservative lower limit of the value indicated above [20-21]. The C_F values for the M group, together with the two available for the S group, although also affected by scatter, are on average distinctly greater than those of the C-L group.

Table 4.3 Summary of Cl^- concentration measurements

Specimen Number	Polarization Voltage (mV_{SCE})	t_A (Days)	Powder Mass (g)	C_S (kppm)	Powder Mass (g)	Measured C_F (kppm)	Corrected C_F (kppm) **	Powder Mass (g)	C_B (kppm)	C_F/C_B
C5	-100	62	3.50	10.19	1.14	5.93	5.62	1.53	0.15	37.0
			2.19	10.28	1.16	5.52	5.20	1.82	0.13	39.7
C1	-100	65	1.43	11.22	1.35	2.10	1.78	1.75	0.17	10.7
			1.10	11.18	1.75	4.88	4.42	2.15	0.07	66.0
			-	-	1.93	4.95	4.48	1.87	0.16	28.9
C9	-100	77	2.66	14.29	2.13	3.78	3.27	2.41	0.20	16.7
			2.01	12.55	2.00	3.91	3.42	1.97	0.20	17.3
Average of C	-100	68	2.15	11.62	1.64	4.44	4.03	1.93	0.15	30.9
L2	-200	38	0.00	-	1.00	1.95	1.02	0.53	* 0.14	7.3
L10	-200	76	3.00	12.49	2.07	4.78	4.61	2.85	0.13	35.7
			1.84	12.34	2.12	2.89	2.75	2.25	0.20	13.9
L6	-200	105	4.12	9.01	2.65	2.97	2.88	2.61	0.09	31.3
Average of L	-200	73	2.99	11.28	1.96	3.15	2.81	2.06	0.14	22.1
M3	-300	91	2.41	10.54	2.11	4.43	4.06	2.19	0.10	39.4
			-	-	2.48	3.63	3.28	3.07	0.08	40.0
M11	-300	157	2.68	13.68	2.28	6.63	6.37	2.29	0.13	47.5
M7	-300	195	2.40	14.25	2.11	8.13	7.85	3.75	0.16	50.0
Average of M	-300	148	2.50	12.82	2.24	5.70	5.39	2.83	0.12	44.2
S4	-400	118	1.62	14.24	2.18	6.02	5.53	3.07	0.08	72.8
S8	-400	245	2.45	13.69	2.30	8.50	8.43	2.36	0.26	32.7
Average of S	-400	182	2.04	13.97	2.24	7.26	6.98	2.71	0.17	52.7

*Value estimated as indicated in text.

**Corrected C_F values were obtained as detailed in Appendix C

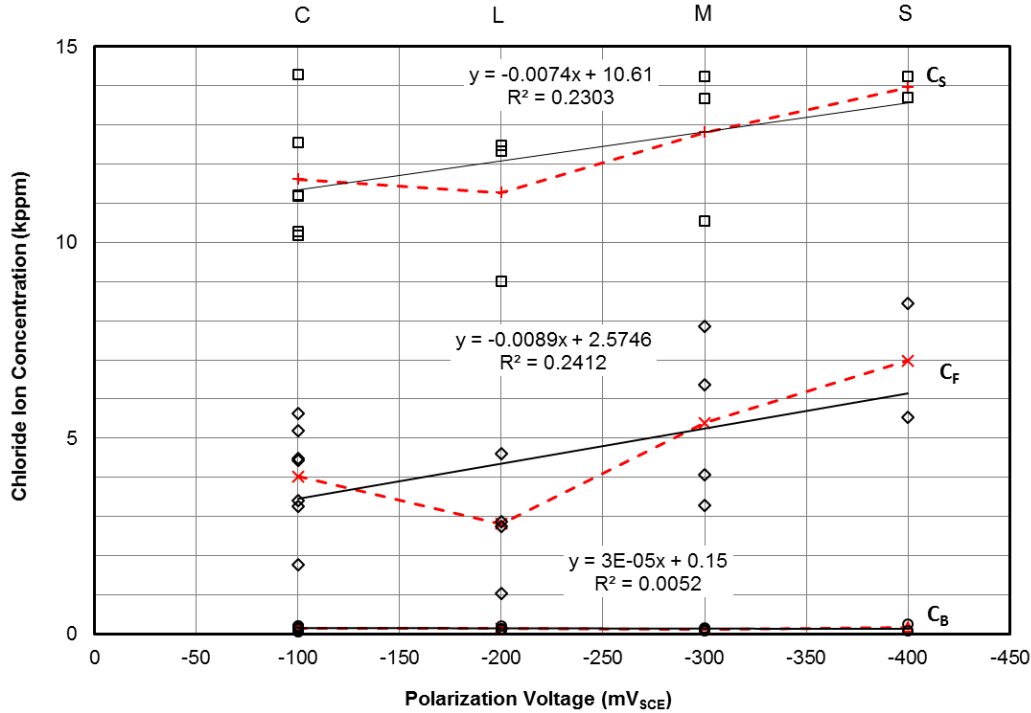


Figure 4.6 Development of C_S , C_F , and C_B with polarization voltage. Red lines indicate averages. Trend lines included for visual speculative evaluation but no functional relationship is implied.

The high scatter of the data observed here is not atypical of the results from other investigations. To put the present findings in the context of prior data, the results obtained here were converted in $C_F\%$ by weight of cement (per Table 3.1) and plotted together with those of earlier investigations. The comparison chart is shown in Figure 4.7, with the red dots representing the C_T values from this work. The present data follow the general trend of the results from the other experiments, with most of the points scattered between the lower and upper limit of prior data. In this context, the present results are consistent with historical reports that have been used a general description of the extent of threshold enhancement on application of cathodic polarization.

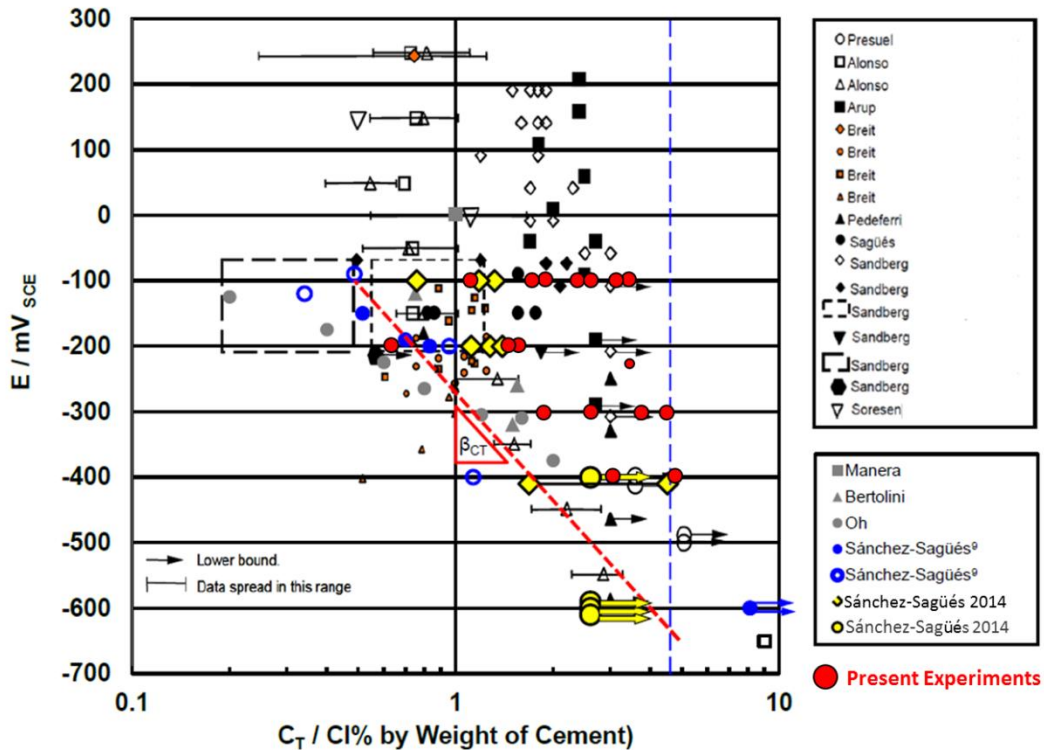


Figure 4.7¹ C_T obtained from this experiment compared to other experiments. The red symbols are C_T obtained in this experiment, while the base graph was taken from the work by Sanchez [20]. The red dashed line represents a proposed boundary to conservatively describe improvement of chloride threshold on cathodic polarization [21].

Important to the objective of this investigation, while in the present work the average Cl^- content of the concrete next to the front steel surface (C_F) increased with cathodic polarization level (which would favor an intrinsic mechanism hypothesis), the increase was not strongly defined as it was affected by the aforementioned marked scatter. An interesting observation however is how the ratio C_F/C_B varies with polarization voltage as seen in Table 4.2. Figure 4.8 shows the plot of C_F/C_B ratio versus polarization voltage. For the specimens polarized at -300 mV_{SCE} and for the one at -400 mV specimen

¹ Reproduced with permission from NACE International, Houston, TX. All rights reserved. Andrea N. Sánchez, *Chloride Corrosion Threshold Dependence on Steel Potential in Reinforced Concrete* Paper No. 4118, Corrosion 2014, 2014, NACE International, San Antonio. © NACE International 2017

for which data were available, the average value clearly increased. Under this metric, which concerns the results of parallel tests on both sides of the specimen, the need for greater chloride levels to activate specimens at greater cathodic polarization becomes

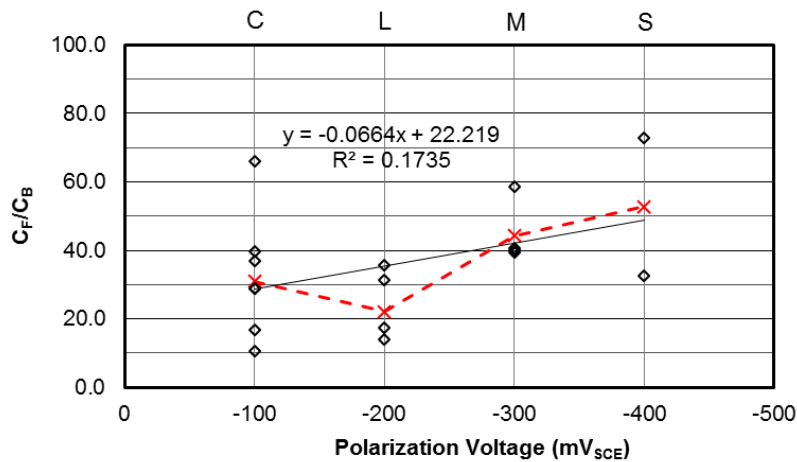


Figure 4.8 C_F/C_B ratio versus polarization voltage. Red line indicates averages. Trend line included for visual speculative evaluation but no functional relationship is implied.

somewhat better defined, again consistent with a dominant intrinsic mechanism.

Finally, it should be noted that the chloride measurements were total chloride measurements, and not values of chloride for only the pore water [24]. Future work should attempt to evaluate free chloride as well as an added means to assess the relative importance of the two mechanisms considered here.

4.4 Visual Observations of Corrosion Damage

Appendix E records the visual appearance of the corrosion damage on the front side of the steel of each of the specimens examined to date. As shown there, with the exception of M7 and S8 corrosion was usually limited to a small fraction of the ~140 cm² front surface area of the specimens, with the rest of the front surface (as well as of the

entire back surface) essentially in the initial passive condition. The size of the corroding spot however tended to be greater for the specimens that had been polarized to the most negative potentials. The reason for this increase is unclear at present, although it may be speculated that as soon as a specimen activated, corrosion would be expected to proceed at a fast pace due the chloride content being greater in the specimens that had aged the most before activation. The significance of this information, provided here for completeness, will be examined in follow up work.

4.5 Summary Remarks on Extrinsic vs Intrinsic Mechanisms

Our study, for the first time to the author's knowledge, obtained simultaneous pore water pH estimates and concrete chloride levels in a systematic evaluation of a C_{prev} system. The results favor to some extent a dominant intrinsic mechanism interpretation, while the evidence in support of a dominant extrinsic mechanism remains elusive. The nominal pH measurements were not differentiated enough, within the experimental scatter, to identify any trend with the applied cathodic polarization level that would support a dominant extrinsic mechanism interpretation. In contrast, the C_F results showed a tendency to increase with increased cathodic polarization level, which would support an intrinsic mechanism interpretation. Nevertheless, due to the natural scatter of the data, the results do not present any evidence strong enough to rule out a possibly dominant extrinsic mechanism. Future development of more precise pH and chloride content measurements, and a wider test matrix to better cancel random errors, may help elucidate this issue. Immediate follow up work will consist of fully characterizing the information obtained from the entire test specimen array (anticipating that activation of the remaining S specimen will occur shortly), further analysis of the corrosion region size data, and combining examination of the results with electrochemical model projections based on alternative working hypotheses.

CHAPTER 5: CONCLUSIONS

1. The experimental data confirm the general expectation that concrete reinforcement benefits from cathodic polarization, as the specimens polarized at high cathodic polarization voltage tended to have higher exposure duration at the time of activation.
2. The pH and chloride ion concentrations obtained in this study favor to some extent a dominant intrinsic mechanism (i.e. due mainly to local interfacial polarization) interpretation, while the evidence in support of a dominant extrinsic mechanism (i.e. due mainly to polarization current-induced concentration changes) interpretation remains elusive. Further experiments and analysis including physical modeling of the system are needed to better resolve this issue.
3. The newly developed ISL method is shown to be capable of obtaining nominal pH values of concrete pore water at steel-concrete interfaces, although with considerably high variability in results and some tendency for systematic bias. Further tests shall be done to refine and improve this method.

REFERENCES

- [1] G. Koch, J. Varney, N. Thompson, O. Moghissi, M. Gould, J. Payer, *International Measures of Prevention, Application, and Economics of Corrosion Technologies Study*, NACE International Impact Study, 2016.
- [2] M.F. Montemor, A.M.P. Simões, M.G.S. Ferriera, *Chloride-induced corrosion on reinforcing steel: from the fundamentals to the monitoring techniques*, *Cement and Concrete Composites*, 2003, Vol. 25, pp. 491-502
- [3] R.R. Hussain, *Passive Layer Development and Corrosion of Steel in Concrete at the Nano Scale*, *Civil and Environmental Engineering*, 2014, Vol.4, pp 1-4.
- [4] K.Y. Ann, H. Song, *Chloride Threshold level for Corrosion of Steel in Concrete*, *Corrosion Science*, 2007, Vol. 49, pp. 4113-4133
- [5] M. Dugarte, A.A. Sagüés, K. Williams, *Cathodic Prevention for Reinforcing Steel in Cracked Concrete of Chloride Contaminated Structures*, Paper No. 6102, *Corrosion 2015*, 2015, NACE International, Houston.
- [6] P. Pedferri, *Cathodic Protection and Cathodic Prevention*, *Constriction and Building Materials*, 1996, Vol. 10, pp. 391-402
- [7] G.K. Glass, J.R. Chadwick, *An investigation into the mechanisms of protection afforded by a cathodic current and the implications for advances in the field of cathodic protection*, *Corrosion Science*, 1994, Vol. 36, pp. 2193-2209
- [8] G.K. Glass, A.M. Hassanein, *Surprisingly Effective Cathodic Protection*, *Journal of Corrosion Science and Engineering*, Vol. 4, Paper 7, 2003
- [9] G.K. Glass, J.Z. Zhang, N.R. Beunfeld, *Chloride Ion Barrier Properties of Small Electric Fields in the Protection of Steel in Concrete*, *Corrosion*, 1995, Vol. 51, pp. 721-726
- [10] G.K. Glass, A.M. Hassanein, N.R. Beunfeld, *Cathodic Protection Afforded by an Intermittent Current Applied to Reinforced Concrete*, *Corrosion Science*, 2001, Vol. 43, pp. 1111-1131

- [11] L. Li, A.A. Sagüés, *Chloride Corrosion Threshold of Reinforcing Steel in Alkaline Solutions—Cyclic Polarization Behavior*, Corrosion, 2003, Vol. 58, pp. 305-316
- [12] S.E. Hussain, Rasheeduzzafar, A. Al-Musallam, A.S. Al-Gahtani, *Factors Affecting Threshold Chloride for Reinforcement Corrosion in Concrete*, Cement and Concrete Research, 1995, Vol. 25, pp.1543-1555
- [13] H. Song, C. Lee. K.Y. Ann, *Factors Influencing Chloride Transport in Concrete Structures Exposed to Marine Environment*, Cement and Concrete Composites, 2008, Vol. 2008, pp. 113-121
- [14] M.G. Fontana, *Corrosion Engineering*, 2005, McGraw-Hill Education
- [15] J.B. Vrable, *Galvanic Corrosion of Reinforcing Steel Exposed to Concrete and Water*, Materials Performance, 1982, Vol. 21, pp. 51-52
- [16] P.Sandberg, *Factors affecting the chloride thresholds for uncracked reinforced concrete exposed in a marine environment. Part I: Field exposure tests of reinforced concrete*, Concrete Science and Engineering, 1999, Vol.1, pp. 92-98
- [17] P.Sandberg, H.E. Sørensen *Factors affecting the chloride thresholds for uncracked reinforced concrete exposed in a marine environment. Part II Laboratory- and field exposure of corrosion cells*, Concrete Science and Engineering, 1999, Vol. 1, pp.99-101
- [18] L. Li, A.A. Sagüés, *Chloride Corrosion Threshold of Reinforcing Steel in Alkaline Solutions Open-Circuit Immersion Tests*, Corrosion, 2001, Vol. 57, pp. 19-28
- [19] C. Alonso, M. Castellotte, C. Andrade, *Chloride Threshold Dependence of Pitting Potential of Reinforcements*, Electrochimica Acta, 2002, Vol. 47, pp. 3469-3481
- [20] A.N. Sanchez, A.A. Sagüés, *Chloride Corrosion Threshold Dependence on Steel Potential in Reinforced Concrete*, Paper No. 4118, Corrosion 2014, 2014, NACE International, San Antonio
- [21] A.N. Sanchez, A.A. Sagüés, *Chloride Threshold Dependence on Potential in Reinforced Mortar*, Paper No. 1728, Corrosion 2012, 2012, NACE International, Houston
- [22] L. Bertolini, F. Bolzoni, M. Gastaldi, T. Pastore, P. Pedferri, E. Redaelli, *Effects of Cathodic Prevention on the Chloride Threshold for Steel Corrosion in Concrete*, Electrochemical Acta, 2009, Vol. 54, pp. 1452-1463
- [23] L. Bertolini, B. Elsener, P. Pedferri, R. Polder, *Corrosion of Steel in Concrete*, WILEY-VCH, 2004

- [24] L. Cáseres, A.A. Sagüés, S.C. Kranc, R.E. Weyers, *In Situ Leaching Method for Determination of Chloride in Concrete Pore Water*, Cement and Concrete Research, 2006, Vol. 36, pp. 492-503
- [25] *Florida Method of Test for Determining Low-Levels of Chloride in Concrete and Raw Materials*, 2013, Florida Department of Transportation.
- [26] R.S. Barneyback Jr, S. Diamond, *Expression and Analysis of Pore Fluids from Hardened Cement Pastes and Mortars*, Cement and Concrete Research, 1981, Vol.11, pp. 279.285
- [27] C.G. McCarty, E. Vitz, *pH Paradoxes: Demonstrating That It Is Not True That $pH = -\log[H^+]$* , Journal of Chemical Education, 2006, Vol. 83, pp. 752-757

APPENDIX A: LIST OF SYMBOLS

C_T	Chloride threshold
C_{Prev}	Cathodic Prevention
C_S	Chloride ion concentration of concrete in contact with pond solution
C_F	Chloride ion concentration of concrete at front surface
C_B	Chloride ion concentration of concrete at back surface
Cl^-	Chloride ion
D	Diffusion Coefficient
OH^-	Hydroxide Ion
t_A	Exposure duration at the time of activation
t_R	Exposure duration at the time of pond solution removal
t_E	Exposure duration at the time of powder sample extraction

APPENDIX B: CHLORIDE ION CONCENTRATION MEASUREMENT

The process to analyze the concrete powder samples for Chloride ion concentration consists of three parts, the powder extraction, concrete powder digestion, and Chloride ions concentration determination.

The samples were extracted from concrete specimens in the form of concrete powder. The powder was milled from the pond, the front, and the back surface of each specimen. The milling machine equipped with carbide-tipped milling tool was used to mill the surfaces of interest at the speed of roughly 4000 rpm. The depth of cut for front and back surfaces was 0.7 mm, and 1 mm surfaces for pond surfaces. The powder resulting from milling was collected using a combination a vacuum pickup fitted with a container holding two nested coffee filter. Each of the collected powder samples was weighted and kept in an airtight glass container.

In order to transform concrete powder samples into Cl^- solutions, a portion of each powder sample was weighed to 0.0001 gram precision. The Florida D.O.T. FM-516 ^[25] instructions recommend using at least 4 grams of powder for an optimum result. However, this threshold was reduced to 1 gram to allow more measurements to be done, thus sacrificing accuracy for higher data diversity. Each sample was diluted in a 100 ml beaker with 15 ml of deionized water. Then, 25ml of a 5% HNO_3 solution was added into the beaker to help digesting the powder. The resultant solution was boiled on

the heating plate held at approximately 250C until the solution started to boil. After the solution was left to boil for 3 to 5 minutes, the solution was poured into a filtering apparatus that was prepared using vacuum pump and Whatman ® N41 filter paper to filter out the remaining solid particles from the solution. The extract was then diluted into a 50 cc distilled water carrier.

The titration of the extracted Cl⁻ solution was done using either 0.1N or 0.01N AgNO₃ as titrant. The potential measured were converted to Cl⁻ concentration by FDOT Chloride 2011 software.

APPENDIX C: CHLORIDE ION CONCENTRATION CORRECTION

As it could take up to several days from the moment of specimen activation to the moment of powder sample extraction, it is highly likely that the Chloride concentration of the concrete at the front surface (see section 3.8) on the date of extraction (C_{FE}) would be slightly higher than the concentration at the date of activation (C_{FA}). This is due to the continuing diffusion of Chloride ions from the concrete at the pond surface to that in the front surface. This situation is explained graphically in Figure C.1, where t_A , t_R and t_E are as defined in section 3.7 and 3.8.

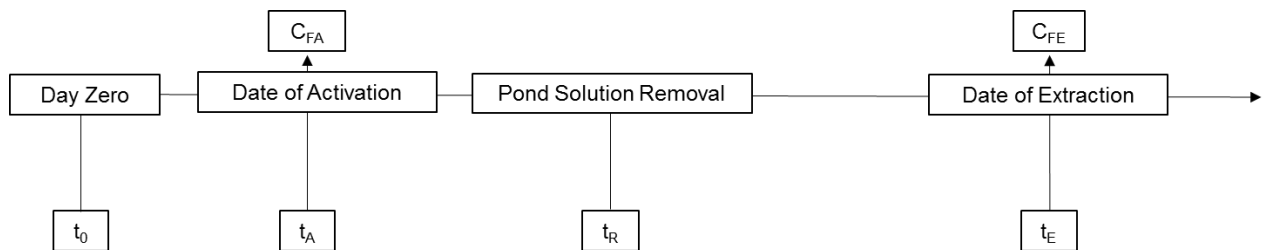


Figure C.1 Diagram showing time lag between t_A and t_E . The diffusion that occurred during the period $t_E - t_A$ increased C_{FA} up to C_{FE}

In order to develop a correction factor to apply to C_{FE} to obtain an estimate of C_{FA} , the following assumptions and simplifications were made.

1. The Chloride concentration of the concrete at the pond surface C_s was considered to be constant not only throughout the actual ponding period, but also

2. during the brief interval between removal of the solution and extraction of the powder sample ($t_R - t_E$).
3. Chloride transport in the concrete proceeded by a simple Fickian diffusion process with an effective diffusion coefficient D that was spatially independent, and with the concrete treated as a uniform medium.
4. Diffusion in the zone between the pond and the front surfaces was treated as a simple one-dimensional problem.
5. Chloride profile evolution during the period between the period t_A to t_E proceeded the same as it has been during the period between day zero and the date of activation; in other words the diffusion coefficient was treated as being time-invariant. 5
6. The native chloride content of the concrete C_0 was assumed negligible.
7. Implicit in the above treatment is the working assumption that the chloride profile on the sample before polarization interruption could be described as having happened by a simple diffusional process. That would have been incorrect if an extrinsic mechanism were dominant. However, as the present procedure is a secondary correction pertaining to a short period of time, the potential error resulting from that assumption not being correct was considered to be secondary as well.

With the above assumptions, we can apply Fick's second law to describe the Chloride profile evolution at the steel-concrete interface. The one-dimensional form of Fick's second law is as follows.

$$\frac{\partial C}{\partial t} = D \frac{\partial^2 C}{\partial x^2} \quad (C.1)$$

where C is Chloride ion concentration (function of x and t) , t is time since the beginning of exposure, D is the diffusion coefficient, and x is the distance within concrete as measured from the concrete-pond solution interface. The distance from the pond to the front surfaces (the concrete cover thickness) is designated as x_c , The boundary conditions per the above statements are $C_s=C(t,0)=\text{constant}$; $C(x,0)=C_0=0$; and no flux at the front surface: $\partial C/\partial x|_{x=x_c} = 0$.

Numerical solution to Fick's second law can be obtained using finite difference method. By dividing the time of exposure t into small periods Δt , and dividing the distance x into intervals Δx , we define the quantity i and j as following.

$$j = \frac{t}{\Delta t} \quad (\text{C.2})$$

$$i = \frac{x}{\Delta x} \quad (\text{C.3})$$

In other words, j and i are simply the number of intervals Δt and Δx that make up the total t and x respectively. Since j also represents time, it shall be referred to as normalized time T from this point onward.

In case of time-dependent diffusion, the theoretical concentration $C_{i,j}$ depends on both time and distance; thus making it difficult to obtain the solution. Fortunately, we can simplify the problem with the following approximations.

$$\frac{\partial C}{\partial x} \approx \frac{C_{i+1,j} - C_{i-1,j}}{2\Delta x} \quad (\text{C.4})$$

$$\frac{\partial^2 C}{\partial x^2} \approx \frac{C_{i+1,j} + C_{i-1,j} - C_{i,j}}{\Delta x^2} \quad (\text{C.5})$$

$$C_{i,j+1} \approx C_{i,j} + \left. \frac{\partial C}{\partial t} \right|_{i,j} \Delta t \quad (\text{C.6})$$

Then, from Fick's second law, it can be demonstrated that by choosing Δx and Δt that satisfy the following condition;

$$2D \frac{\Delta t}{\Delta x^2} = 1 \quad (\text{C.7})$$

the quantity $C_{i,j}$ can be determined by the following equation.

$$C_{i,j} \approx \frac{C_{i-1,j-1} + C_{i+1,j-1}}{2} \quad (\text{C.8})$$

With equation C.8, it is possible to obtain a plot of $C_{i,j}$ versus normalized time. Here, i is chosen to be equal to 20 while x equals to 20 mm; the distance from pond surface to the front surface. This reduces the problem from 2 variables to 1 variable,

The theoretical concentration $C_{i,j}$ was normalized by dividing it by the experimentally obtained concentration of the pond surface C_s . We then constructed the plot of $C_{i,j}/C_s$ at $i=20$ for $j=0$ to $j=1000$. The resultant plot is shown in Figure C.3.

To obtain C_{FA} from the experimentally measured value C_{FE} , we divided it by its respective pond surface chloride concentration C_s . This would yield the C_{FE}/C_s ratio, which can be inserted into our theoretical model to determine the associating normalized time. Since this value of normalized time is analogous to t_E , it was given the symbol T_E . For the same reason, the normalized time associating with C_{FA} was given a symbol T_A .

At this point, it can be established that the ratio T_A/T_E must be equal to the ratio t_E/t_A . Therefore, the value of T_A can be obtained by simply multiplying T_E by the ratio t_E/t_A . We can now use this value of T_A to determine C_{FA} from our theoretical model. The summary of this process is shown in Figure C.2, and the summary of the values obtained from this process is shown in Table C.1. In addition to C_{FA} , this can also estimate the coefficient of diffusion (D) based on the relationship in equation C.7. The values to the

estimated D are shown in the rightmost of Table C.1. Those values are consistent with the diffusivity normally expected from a high water/cement ratio concrete as the one used here [20]. Please note that in the main text of this thesis, C_{FA} was denoted simply by C_F .

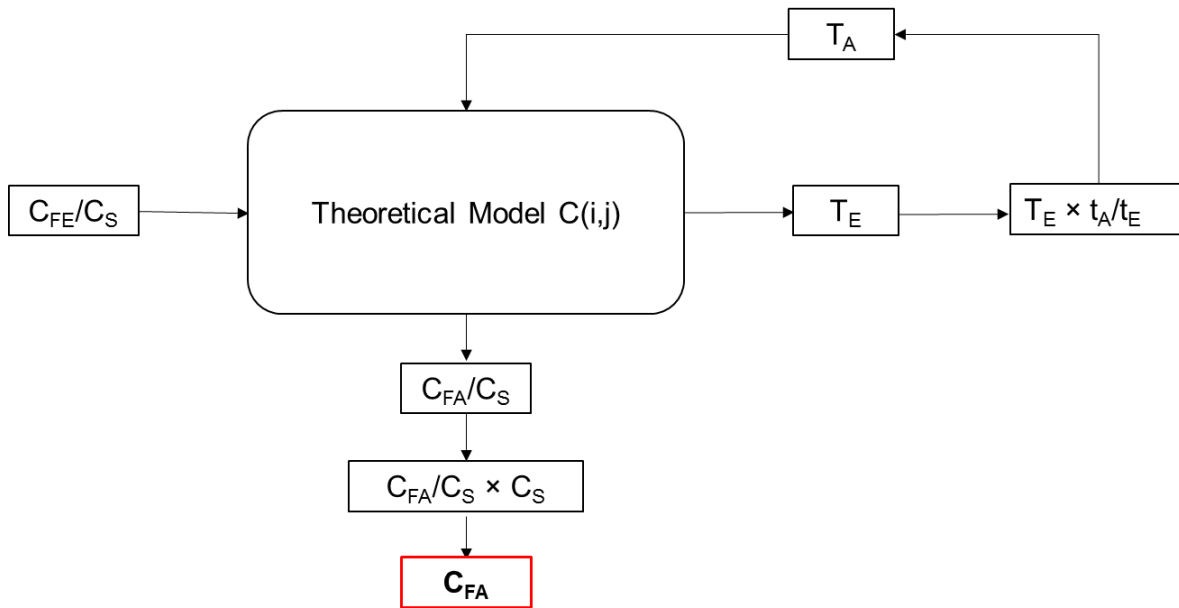


Figure C.2 Summary of the process to obtain C_{FA} from C_{FE}

Table C.1 Summary of C_F values at the time of activation

Specimen No.	C_{FE} (ppm)	C_s (ppm)	C_{FE}/C_s	Theoretical C/C_s	T_E	t_A (Days)	t_E (Days)	t_A/t_E	T_A	C_{FA}/C_s	C_{FA} (ppm)	D (cm ² /s)
C1	2100	11218	0.19	0.19	149	65	71	0.92	136	0.16	1778	1.2E-07
C1	4884	11218	0.44	0.44	276	65	71	0.92	253	0.39	4421	2.2E-07
C1	4948	11218	0.44	0.44	279	65	71	0.92	255	0.40	4480	2.3E-07
C5	5933	10188	0.58	0.58	378	62	66	0.94	355	0.55	5623	3.3E-07
C5	5516	10188	0.54	0.54	347	62	66	0.94	326	0.51	5203	3.0E-07
C9	3777	14286	0.26	0.26	184	77	84	0.92	169	0.23	3266	1.3E-07
C9	3909	14286	0.27	0.27	189	77	84	0.92	173	0.24	3418	1.3E-07
L2	1952	11744	0.17	0.17	139	38	51	0.75	104	0.09	1024	1.6E-07
L6	2973	9008	0.33	0.33	217	105	107	0.98	213	0.32	2877	1.2E-07
L10	4777	12492	0.38	0.38	245	76	78	0.97	239	0.37	4608	1.8E-07
L10	2886	12492	0.23	0.23	169	76	78	0.97	165	0.22	2748	1.3E-07
M3	4428	10537	0.42	0.42	267	91	98	0.93	248	0.39	4058	1.6E-07
M3	3628	10537	0.34	0.34	224	91	98	0.93	208	0.31	3283	1.3E-07
M7	8132	14248	0.57	0.57	369	195	203	0.96	354	0.55	7846	1.1E-07
M11	6631	13679	0.48	0.48	307	157	163	0.96	296	0.47	6370	1.1E-07
S4	6024	14238	0.42	0.42	268	118	127	0.93	249	0.39	5535	1.2E-07
S8	8501	13693	0.62	0.62	411	245	247	0.99	408	0.62	8427	9.6E-08

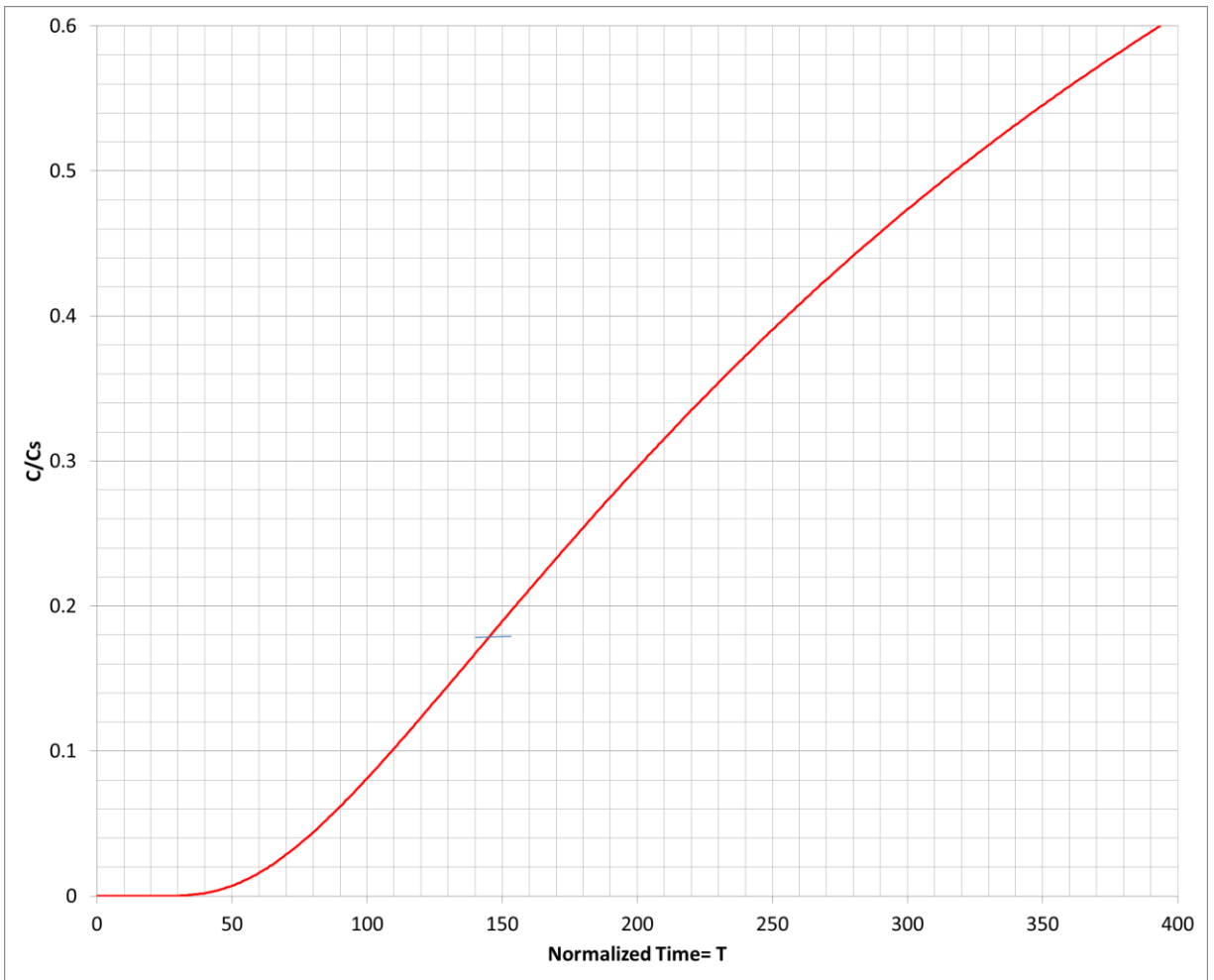


Figure C.3 Plot of C/C_s versus normalized time

APPENDIX D: CONFIRMATORY NYQUIST PLOTS

As indicated in section 3.7, the specimens that had shown signs of corrosion (e.g. a drop in potential, zero current) had to be tested by EIS. All the EIS measurements were taken over the frequency range 1mHz-100 kHz (except for L10 and M11, 10mHz-100 kHz), 3 points per decade, excitation amplitude = 10 mV_{rms}. The datum with the largest absolute value of impedance in each plot corresponds to the corresponding lowest frequency. Results are reported in ohms; for area-normalized results (ohm-cm²) multiply the impedance by 140 cm², which is the surface area of the steel in contact with concrete in the “front” interface and assumed to be receiving most of the excitation current.

Table D.1 Summary of the important EIS parameters

Specimen No.	Open circuit potential at the time of testing (V)	t _A (Days)	Z _{max} (Ohm)	Frequency corresponding to Z _{max} (mHz)
C1	-0.322	65	2.8E+04	1
C5	-0.263	62	6.9E+04	1
C9	-0.320	77	1.9E+04	1
L2	-0.270	38	6.2E+04	1
L6	-0.165	105	1.9E+05	1
L10	-0.304	76	4.3E+04	10
M3	-0.261	91	7.9E+04	1
M7	-0.289	195	7.0E+04	1
M11	-0.378	157	3.2E+04	10
S4	-0.220	118	2.7E+04	1
S8	-0.426	245	2.1E+04	1

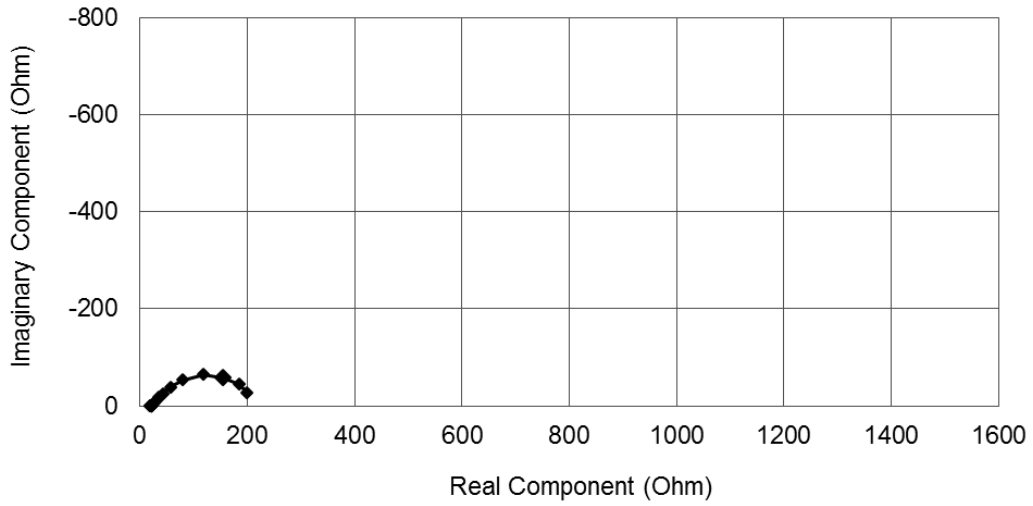


Figure D.1 Nyquist plot of the specimen C1, shown in a comparative scale. The test was done after 65 days of exposure duration. The specimen's open circuit potential at the moment of EIS test was -322 mV

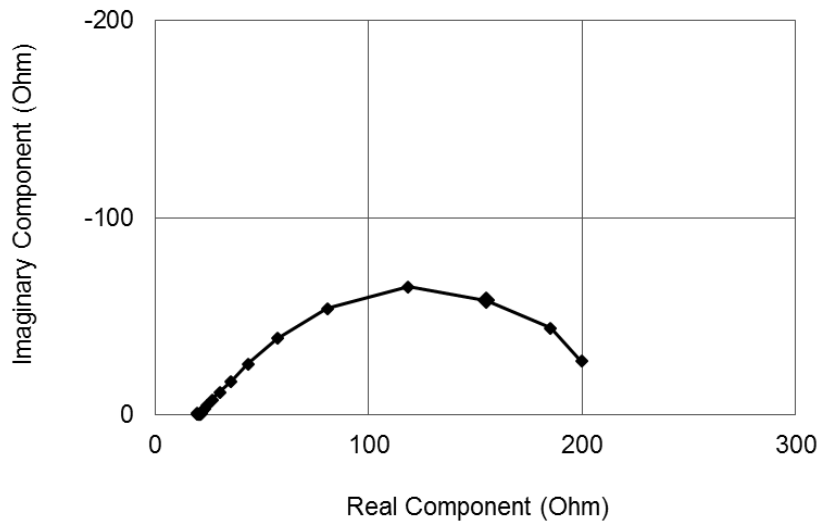


Figure D.2 Close-up look of the Nyquist plot of the specimen C1

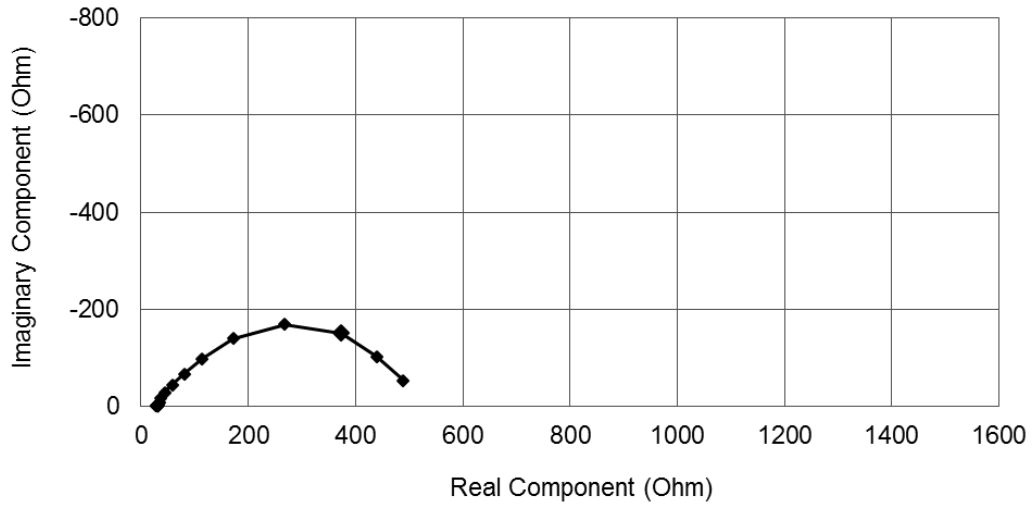


Figure D.3 Nyquist plot of the specimen C5, shown in a comparative scale. The test was done after 62 days of exposure duration. The specimen's open circuit potential at the moment of EIS test was -263 mV

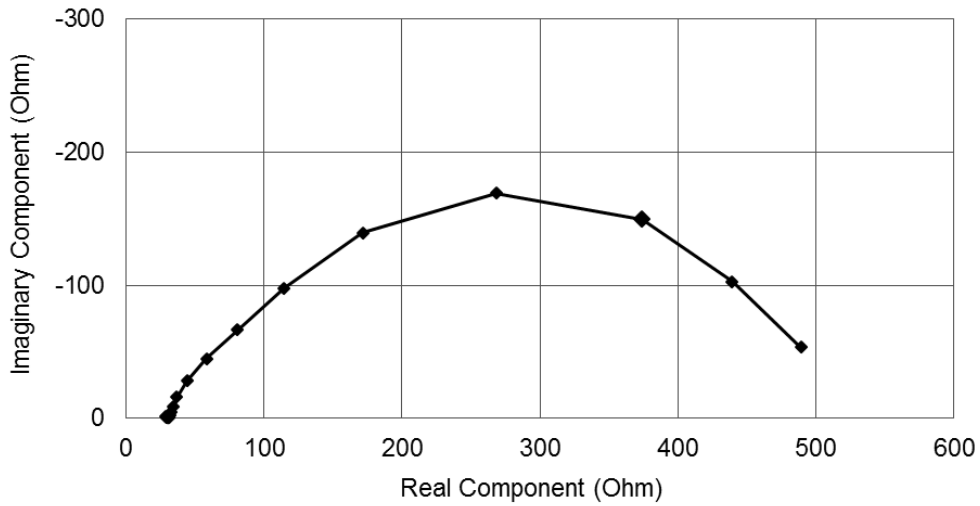


Figure D.4 Close-up look of the Nyquist plot of the specimen C5

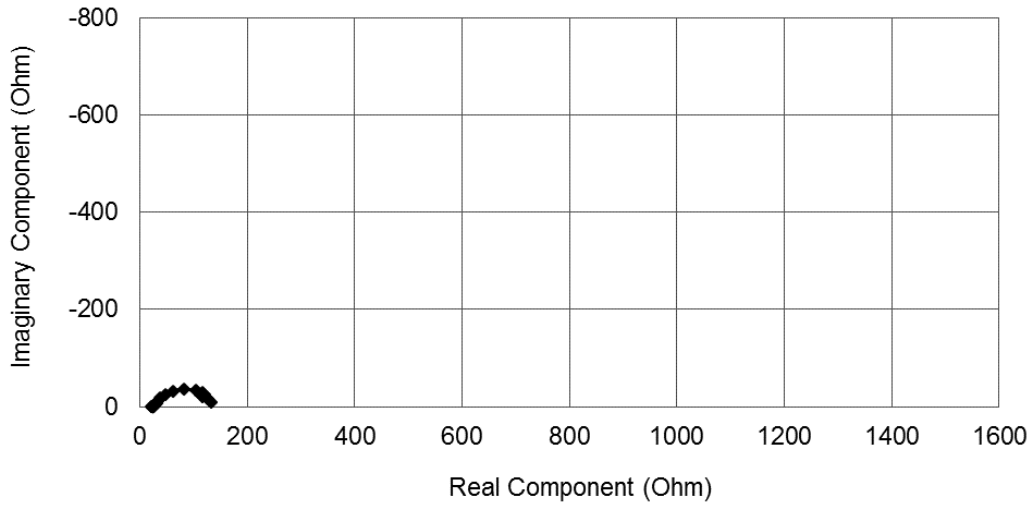


Figure D.5 Nyquist plot of the specimen C9, shown in a comparative scale. The test was done after 77 days of exposure duration. The specimen's open circuit potential at the moment of EIS test was -319 mV

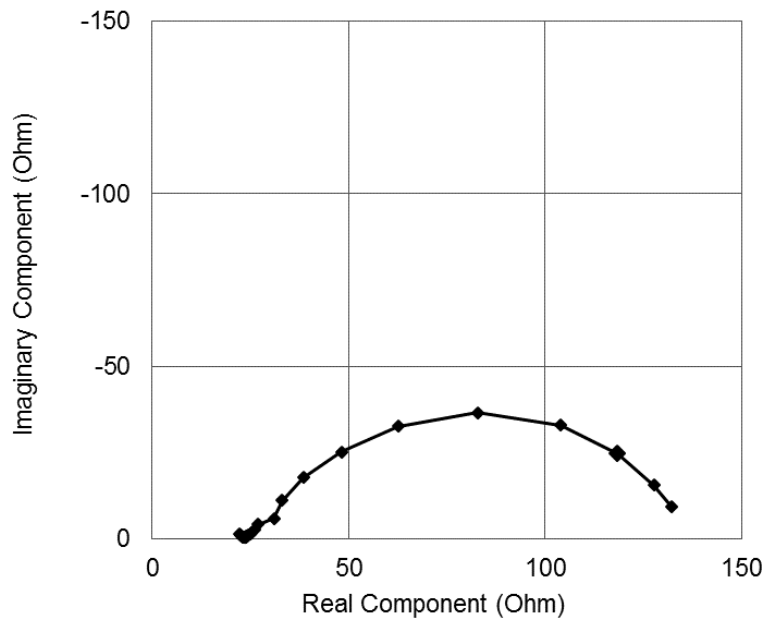


Figure D.6 Close-up look of the Nyquist plot of the specimen C9

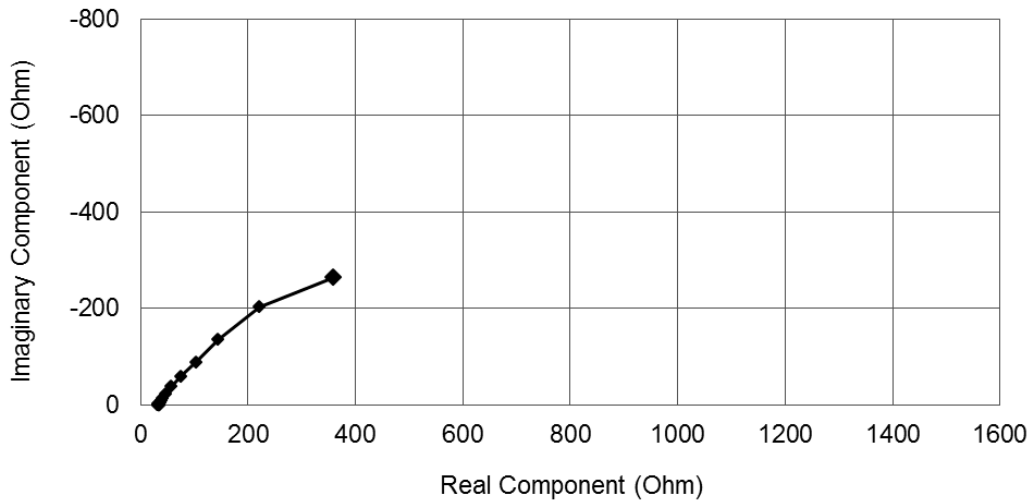


Figure D.7 Nyquist plot of the specimen L2, shown in a comparative scale. The test was done after 38 days of exposure duration. The specimen's open circuit potential at the moment of EIS test was -270 mV

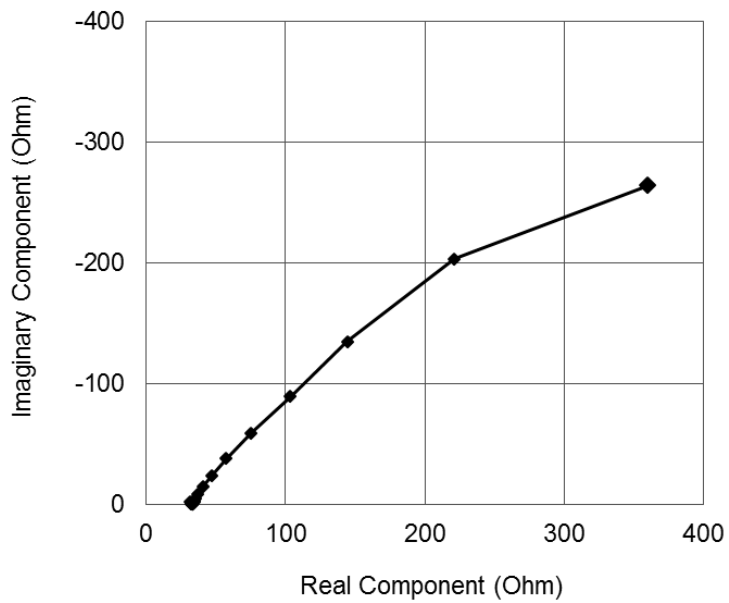


Figure D.8 Close-up look of the Nyquist plot of the specimen L2

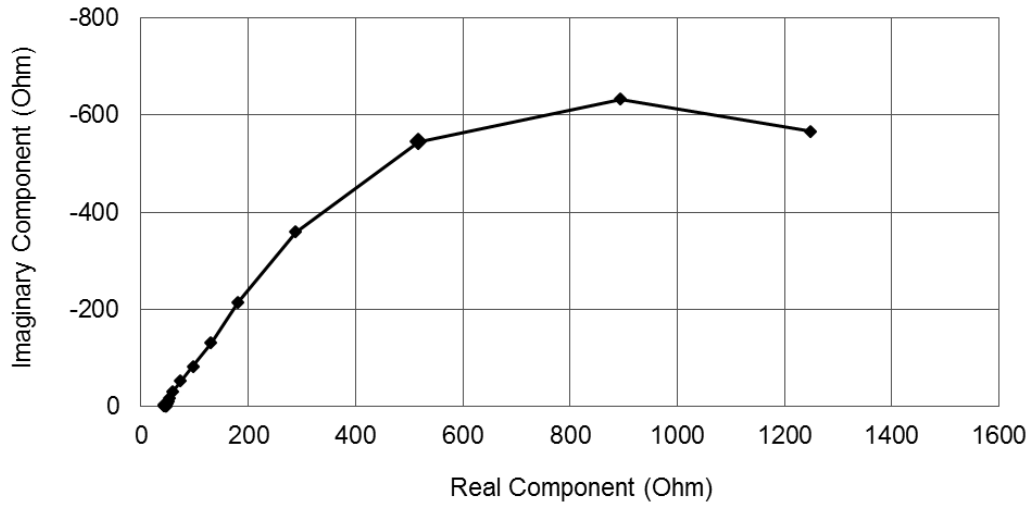


Figure D.9 Nyquist plot of the specimen L6, shown in a comparative scale. The test was done after 105 days of exposure duration. The specimen's open circuit potential at the moment of EIS test was -165 mV

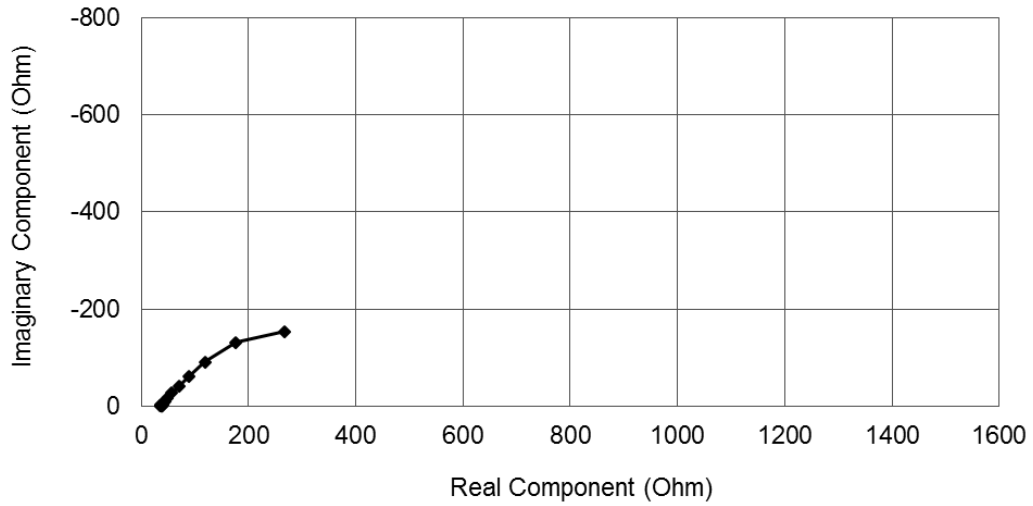


Figure D.10 Nyquist plot of the specimen L10, shown in a comparative scale. The test was done after 76 days of exposure duration. The specimen's open circuit potential at the moment of EIS test was -165 mV

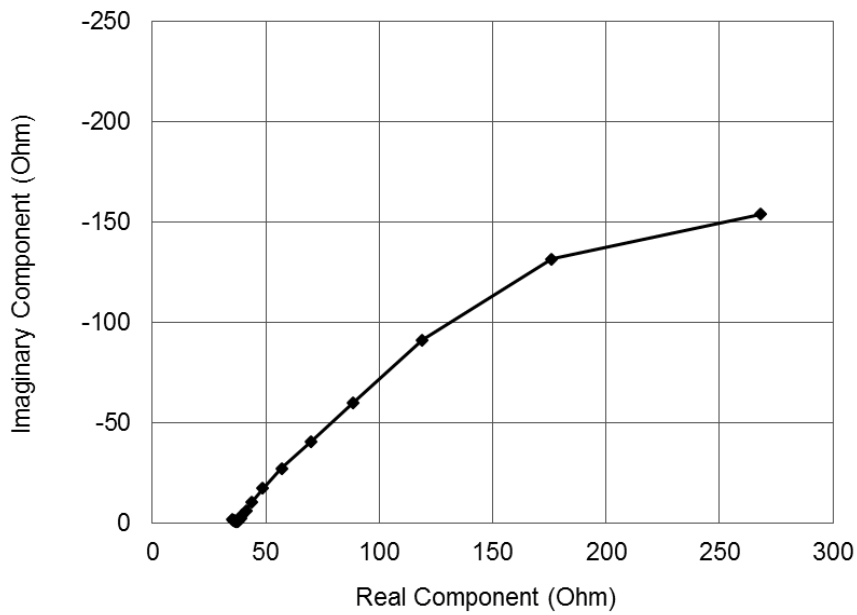


Figure D.11 Close-up look of the Nyquist plot of the specimen L10

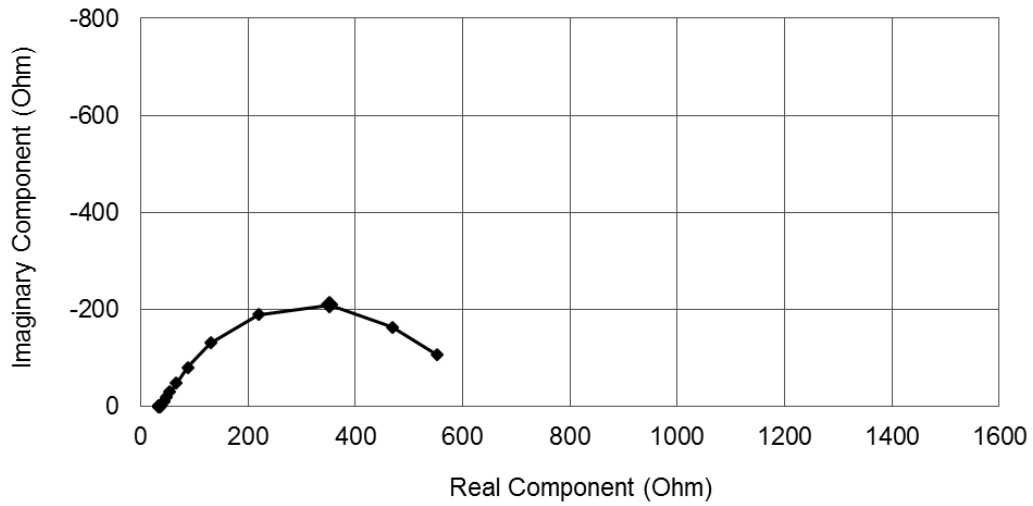


Figure D.12 Nyquist plot of the specimen M3, shown in a comparative scale. The test was done after 91 days of exposure duration. The specimen's open circuit potential at the moment of EIS test was -261 mV

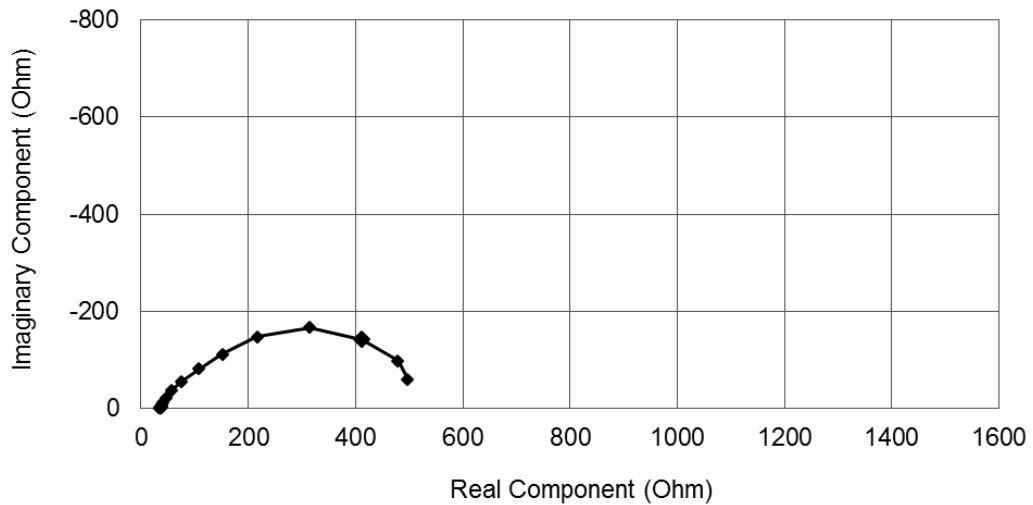


Figure D.13 Nyquist plot of the specimen M7, shown in a comparative scale. The test was done after 195 days of exposure duration. The specimen's open circuit potential at the moment of EIS test was -289 mV

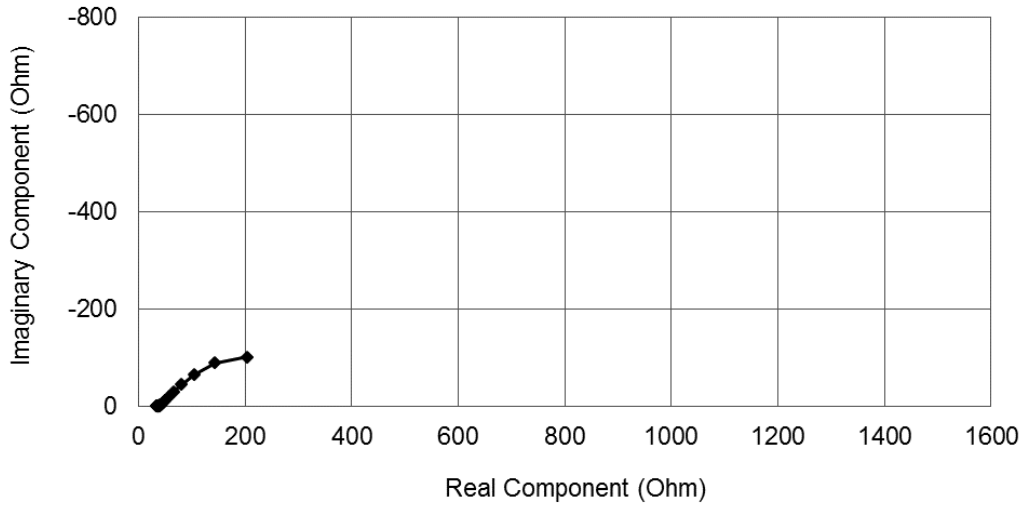


Figure D.14 Nyquist plot of the specimen M11, shown in a comparative scale. The test was done after 157 days of exposure duration. The specimen's open circuit potential at the moment of EIS test was -378 mV

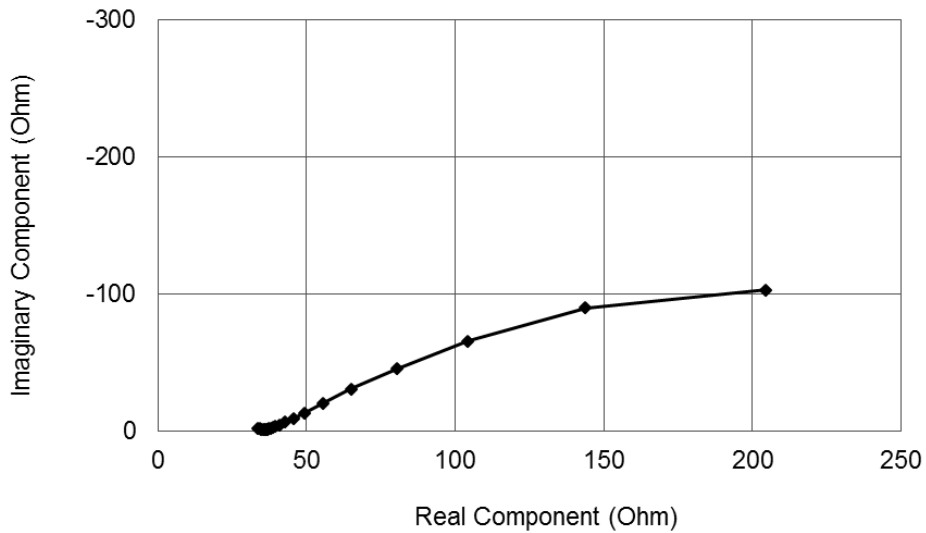


Figure D.15 Close-up look of the Nyquist plot of the specimen M11

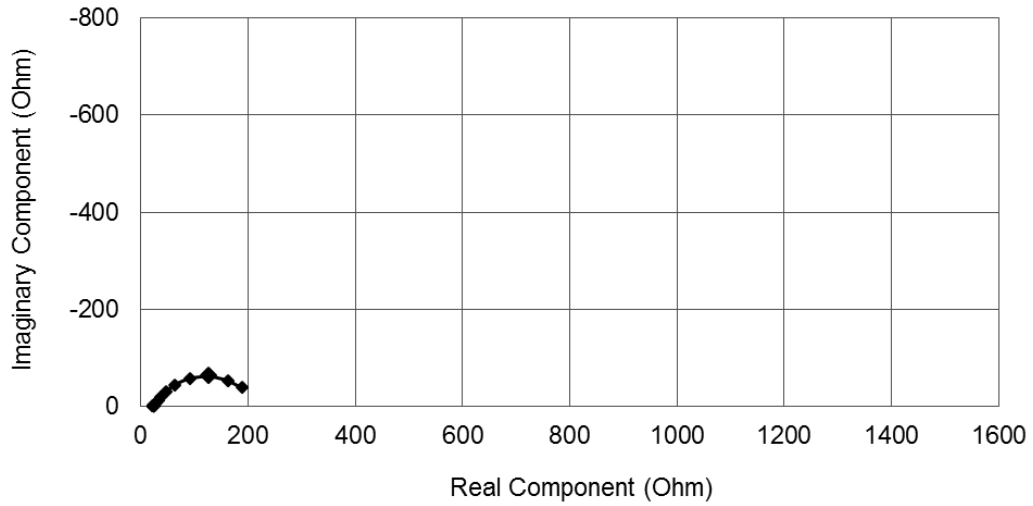


Figure D.16 Nyquist plot of the specimen S4, shown in a comparative scale. The test was done after 118 days of exposure duration. The specimen's open circuit potential at the moment of EIS test was -220 mV

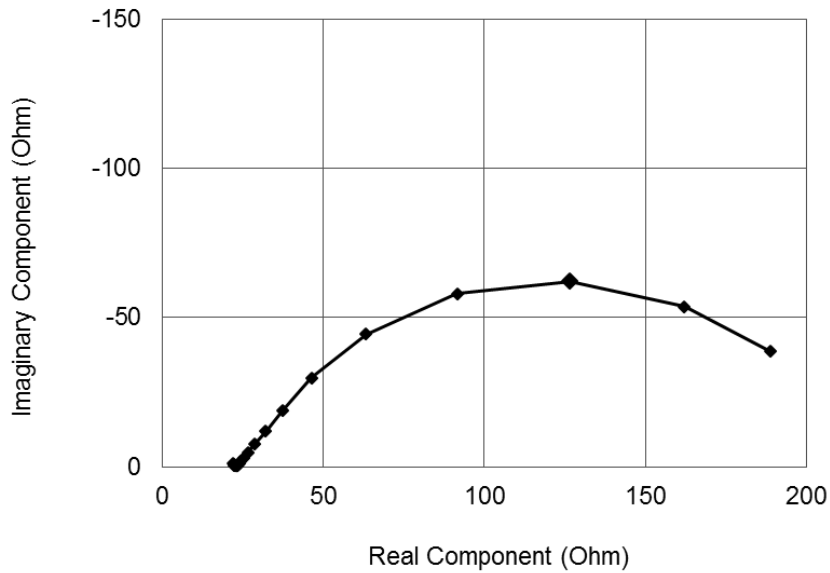


Figure D.17 Close-up look of the Nyquist plot of the specimen S4

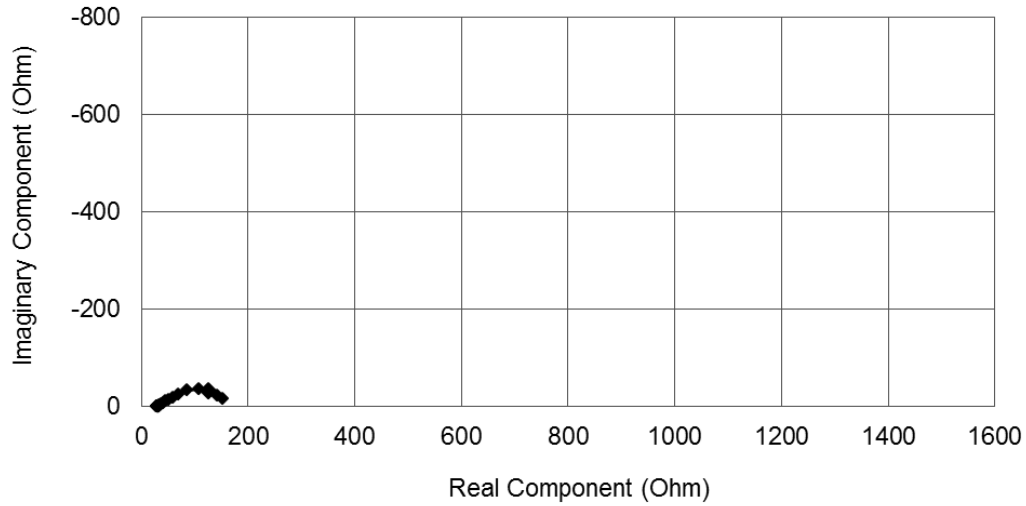


Figure D.18 Nyquist plot of the specimen S8, shown in a comparative scale. The test was done after 246 days of exposure duration. The specimen's open circuit potential at the moment of EIS test was -258 mV

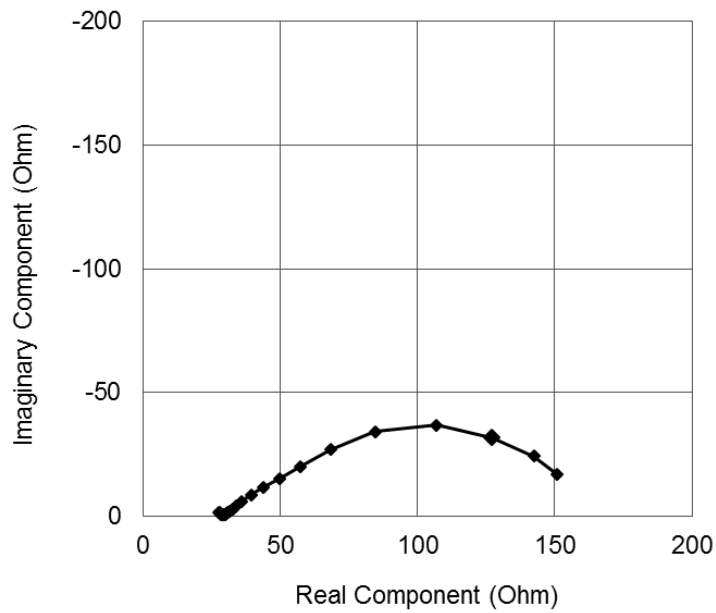


Figure D.19 Close-up look of the Nyquist plot of the specimen S8

APPENDIX E: CORROSION SPOTS ON ACTIVATED SPECIMENS

In this section, we documented the photos of the corrosion spots found on the steel plates and the front surface at the day of demolition. The corrosion spots or areas are circled in red. Table E.1 summarizes the size of the corrosion spots as estimated by a product of their approximate length and width.

Table E.1 Summary of the corrosion spots size

Specimen No.	t_A (Days)	Estimated Area of Corrosion Spots (cm ²)
C1	65	0.5
C5	66	0.8
C9	77	0.5
L2	38	1.1
L6	105	0.8
L10	76	1.3
M3	91	6.4
M7	195	8.8
M11	157	7.2
S4	118	4.6
S8	245	20



Figure E.1 Corrosion spots on the steel-concrete interface of specimen C1.

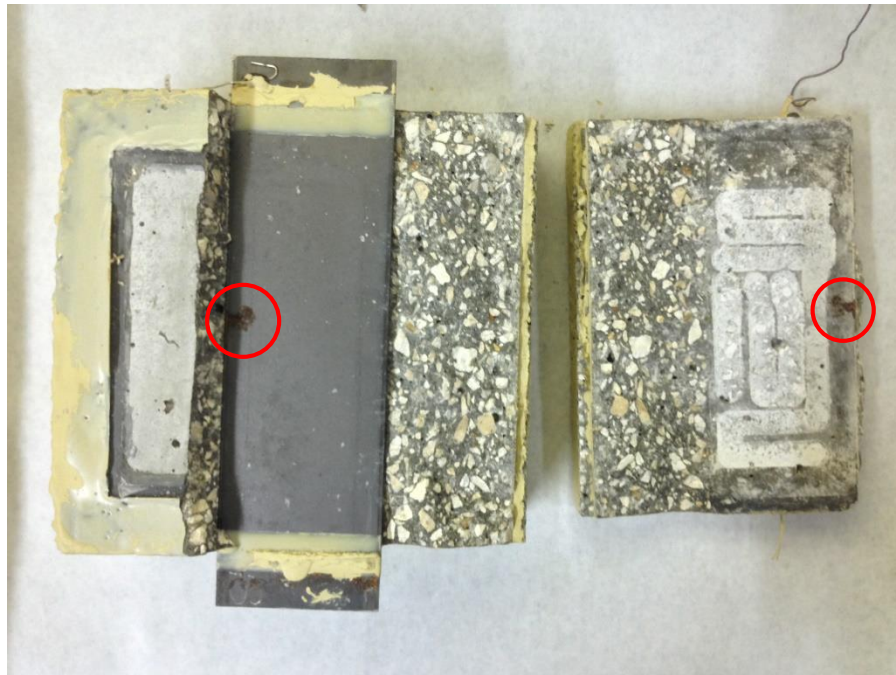


Figure E.2 Corrosion spots on the steel-concrete interface of specimen C5



Figure E.3 Corrosion spots on the steel-concrete interface of specimen C9

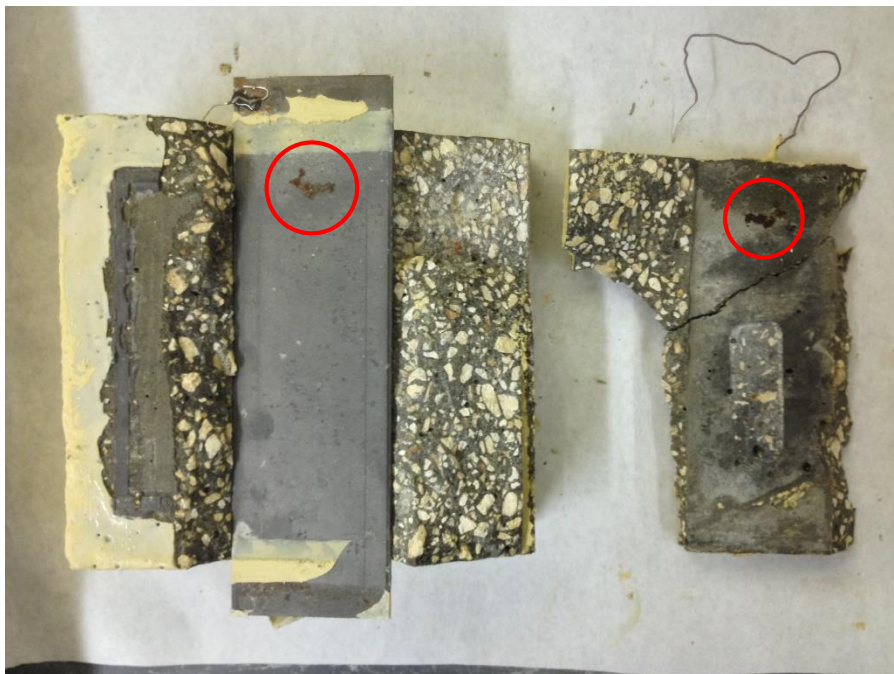


Figure E.4 Corrosion spots on the steel-concrete interface of specimen L2



Figure E.5 Corrosion spots on the steel-concrete interface of specimen L6

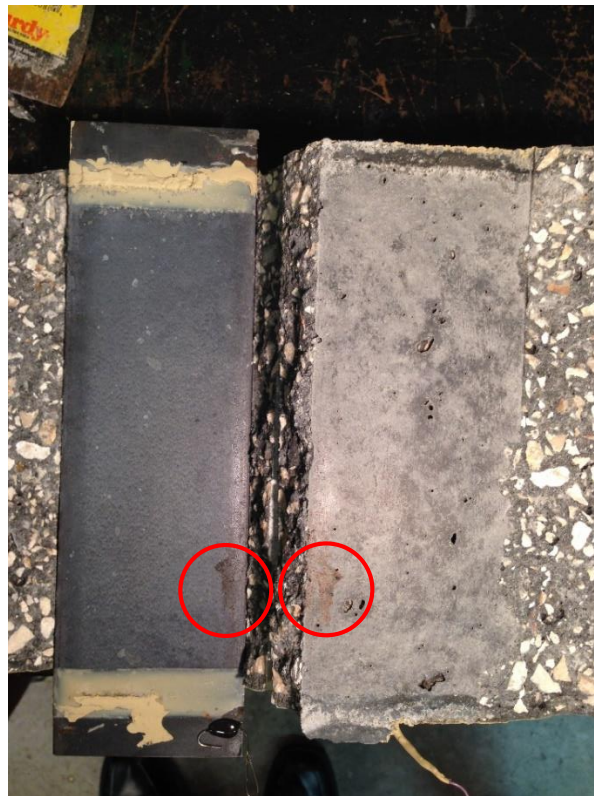


Figure E.6 Corrosion spots on the steel-concrete interface of specimen L10

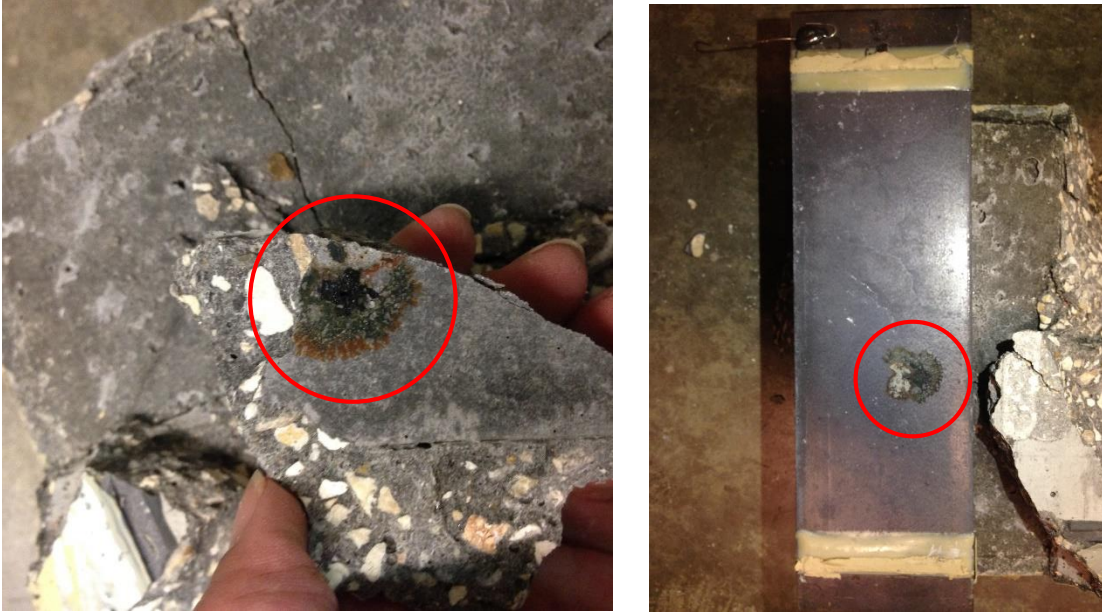


Figure E.7 Corrosion spots on the steel-concrete interface of specimen M3



Figure E.8 Corrosion spots on the steel-concrete interface of specimen M7



Figure E.9 Corrosion spots on the steel-concrete interface of specimen M11



Figure E.10 Corrosion spots on the steel-concrete interface of specimen S4



Figure E.11 Corrosion spots on the steel-concrete interface of specimen S8

APPENDIX F: COPYRIGHT PERMISSION

Figures 4.7 have been reproduced with permission from NACE International, Houston, TX, all rights reserved. Paper no. 4118 was presented at CORROSION/2014, San Antonio, TX. © NACE International 2014.



NACE International
15835 Park Ten Place
Houston, TX 77084
Tel: 281-228-6200
Fax: 281-228-6300

Permission to Reproduce Figures, Photos, and Tables from Copyrighted Works

Date: 3/21/2017
Name: Krittin Rattakham Title: Mr.
Company ("Publisher"): University of South Florida
Address: 4202 E Fowler Ave, Tampa, FL 33620
Tel: (813) 974-2011 Fax: N/A
Email: krittin@mail.usf.edu

Material to be Reproduced ("Work"): Please provide a complete description of the material involved. Include the following elements where applicable: publication name, issue date, page number, figure/photo/table number, paper number, conference name, etc.
Paper No. 4118, "Chloride Corrosion Threshold Dependence on Steel Potential in Reinforced Concrete", NACE 2014, S.A. Texas, page 9, Figure 7

Reproduction Method ("Publication Media"): Please provide a complete description of how and where the Work will be used. Include the following elements as applicable: publication name, issue, circulation, print run, web site address, conference name, presentation time and place, etc.
The figure will be used in a master thesis "Mechanism of Cathodic Prevention of Carbon Steel in Concrete" and submitted to the graduate school of University of South Florida. The results presented in this figure will be compared to those in the thesis.

NACE International ("NACE") hereby grants to "Publisher" the right to publish the Work utilizing the Publication Media described above. The publication right granted herein is limited to the specific Publication Media described above. To the extent the publication of the Work is to occur by an above-specified date, such as in a particular periodical or at a particular conference, the right granted herein shall automatically terminate upon the date of such occurrence, whether or not the Work is actually published. To the extent the Publication Media is a web site, the publication right is limited to publication at the specific web site URL identified above. Any right granted herein is a limited, non-transferable, non-exclusive right. No other rights in the Work are granted herein.

Publisher shall not edit or modify the Work except to meet the style and graphic requirements of the individual media involved.

The Publisher shall include the following notation with any publication of the Work:*

- A. Conference Paper**
Reproduced with permission from NACE International, Houston, TX. All rights reserved. Author(s), Paper NUMBER presented at CORROSION/YEAR, City, State. © NACE International FIRST YEAR OF PUBLICATION.
- B. Journal Article**
Reproduced with permission from NACE International, Houston, TX. All rights reserved. Author(s) name, Article title, Journal title, Vol. no., Issue no., and publication year. © NACE International FIRST YEAR OF PUBLICATION.
- C. Magazine Article**
Reproduced with permission from NACE International, Houston, TX. All rights reserved. Author(s) name, Article title, Magazine title, Vol. no., Issue no., and publication year. © NACE International FIRST YEAR OF PUBLICATION.
- D. Standards**
STANDARDS/TECHNICAL COMMITTEE REPORT NAME, © NACE International YEAR. All rights reserved by NACE. Reprinted with permission. NACE standards are revised periodically. Users are cautioned to obtain the latest edition; information in an outdated version of the standard may not be accurate.

* Modifications to Notations: Other reference wording can be used, but must be approved by NACE in writing *in advance*.

The Publisher shall include full bibliographic citations of or references to the original NACE source, where applicable.

Publisher shall obtain a copy of the original Work directly from NACE International and shall not utilize copies of the Work from other sources, including the author(s).

To the extent the Work is published on a web site as authorized herein, the Work shall be posted in a file format that does not allow the content of the Work to be easily copied from the Web Site or changed.

As between NACE and Publisher, Publisher acknowledges that NACE owns all rights in the Works.

Publisher shall not be entitled to any compensation for its efforts in promoting the Work.

THE WORK IS PROVIDED "AS IS." ALL EXPRESS OR IMPLIED COVENANTS, CONDITIONS, REPRESENTATIONS OR WARRANTIES, INCLUDING ANY IMPLIED WARRANTY OF MERCHANTABILITY OR FITNESS FOR A PARTICULAR PURPOSE OR CONDITIONS OF ACCURACY, COMPLETENESS OR QUALITY AND THOSE ARISING BY STATUTE OR OTHERWISE IN LAW, ARE HEREBY DISCLAIMED.

IN NO EVENT WILL NACE BE LIABLE FOR ANY DIRECT, INDIRECT, PUNITIVE, SPECIAL, INCIDENTAL OR CONSEQUENTIAL DAMAGES IN CONNECTION WITH OR RELATED TO THIS AGREEMENT (INCLUDING LOSS OF PROFITS, USE, DATA, OR OTHER ECONOMIC ADVANTAGE), HOWSOEVER ARISING.

This Agreement and the rights granted herein may be terminated immediately by NACE upon breach of this Agreement by Publisher. Unless earlier terminated, this Agreement and the rights granted herein will automatically terminate 6 months from the Date set forth above. If the Work has not been published within that time period, a new Agreement must be obtained.

Publisher may not, directly or indirectly, sell, assign, sublicense, lease, rent, distribute, or otherwise transfer this Agreement or any rights granted herein, without the prior written consent of NACE.

If any provision of this Agreement is found to be unenforceable, then this Agreement shall be deemed to be amended by modifying such provision to the extent necessary to make it legal and enforceable while preserving its intent. The remainder of this Agreement shall not be affected by such modification.

This Agreement does not create, and shall not be construed to create, any employer-employee, joint venture or partnership relationship between the parties. No officer, employee, agent, servant or independent contractor of either party shall at any time be deemed to be an employee, servant, agent or contractor of any other party for any purpose whatsoever.

This Agreement shall be governed by, and construed and enforced in accordance with, the laws of the State of Texas, without regard to the choice of law provisions of that State.

This Agreement shall only be effective if signed by authorized representatives of both parties. This Agreement constitutes the entire Agreement between the parties with respect to the subject matter of this Agreement. Any change, modification or waiver hereto must be in writing and signed by authorized representatives of both parties.

Other Terms & Conditions: _____

Publisher hereby requests permission to publish the Work described above and agrees to comply with all Terms and Conditions listed above.

Request submitted by:
Krittin Rattakham
Printed Name
Krittin Rattakham
Title
Mr.
Signature
Date
3/21/2017

Request agreed to by:
Andrea N. Sánchez
Lead Author Printed Name
Andrea N. Sánchez
Lead Author Title
Corrosion Engineer
Lead Author Signature
3/21/2017

Request approved by NACE:
Daniela Freeman
Printed Name
Audience Development Manager
@nace.org
Signature
3/22/2017
Date